Assessing the Ability of Sodium Carboxymethyl Cellulose Oxygen Nanobubbles to Reverse Acute Hypoxia in Isolated Peripheral Blood Lymphocytes

S.NANDHINI

(20PBC014)

Under the guidance of

Dr. E. Nithya

Assistant professor

A Thesis submitted in

Partial fulfilment of the

Degree of Master of Science in Biochemistry

Avinashilingam Institute for Home Science and Higher Education for Women

Coimbatore – 641043

May 2022

Certificate

Assessing the Ability of Sodium Carboxymethyl Cellulose Oxygen Nanobubbles to Reverse Acute Hypoxia in Isolated Peripheral Blood Lymphocytes

S.NANDHINI

(20PBC014)

Thesis submitted to

Department of Biochemistry, Biotechnology and Bioinformatics

Avinashilingam Institute for Home Science and Higher Education for Women

Coimbatore – 641043

In Partial Fulfilment of the requirement for the degree of

Master of Science in Biochemistry

May 2022

Signature of the Guide

31/5/2022

Signature of the Head of the Department

Acknowledgement

ACKNOWLEDGEMENT

I owe a special tribute to **God Almighty** for the opportunity given to take up to complete my work successfully. In addition to the will of supreme divinity, the willingness of many subject experts and erudite scholars to extent their assistance and help for completion of a work plays, indeed a vitally important role.

I express my deep sense of gratitude to all my higher authorities of Avinashilingam Institute for Home Science and High Education for Women, Coimbatore for their immense support.

I take the opportunity of expressing my sincere thanks to **Dr. (Thiru) P.R. Krishna Kumar (Late)** and **Dr. (Thiru) S.P. Thiyagarajan,** Chancellor, Avinashilingam Institute for Home Science for Higher Education for Women, Coimbatore, for providing the opportunity and infrastructure to undertake this investigation.

I immensely thank **Dr. V. Bharathi Harishankar,** Vice Chancellor, Avinashilingam Institute for Home Science and Higher Education for Women, Coimbatore, for providing the entire facilities essential to carry out and complete the study.

I record my sincere thanks to **Dr. S. Kowsalya,** Registrar, Avinashilingam Institue for Higher Education for Women, Coimbatore, for timely help rendered to carry out the work

I express my special gratitude to **Dr. A. Vijayalakshmi**, Dean, School of Biosciences, Professor and Head, Department of Botany, Avinashilingam Institute for Home Science and Higher Education for Women, Coimbatore, for providing the opportunity and timely help rendered to carry the work successfully

I express my reverential thanks to **Dr. P. Lalitha,** Director, Research and Consultancy, Avinashilingam Institute for Home and Higher Education for Women, Coimbatore for their support and encouragement rendered towards the completion of my thesis work.

I record my sincere gratitude to **Dr. Anitha Subash,** Professor and Head, Department of Biochemistry, biotechnology and Bioinformatics, Avinashilingam Institute for Home Science

and Higher Education for Women, Coimbatore, and her immense support and motivation throughout my study.

I owe my indebtedness, profound and deepest thanks to my guide **Dr. E. Nithya,** Assistant Professor, Department of Biochemistry, Biotechnology and Bioinformatics, Avinashilingam Institute for Home Science and Higher Education for Women, Coimbatore, for her incessant guidance, immense tolerance, meticulous care, good support, creative influences, thoughtful advise, steady encouragement, motherly love throughout the research and motivation right from selection of topic and completion of the work effectively and efficiently.

I submit my sincere thanks to all **The Staff Members,** of Department of Biochemistry, Biotechnology and Bioinformatics, Avinashilingam Institute for Home Science and Higher Education for Women, Coimbatore, for lending a helping hand and invaluable guidance during the course of this thesis work.

I place my gratitude to foot of my parents for their immense support and guidance during the course of my study.

I express my sincere heart bound thanks to my friends, Department of Biochemistry, Biotechnology and Bioinformatics, for giving an affectionate advice, unconditional love and incredible support for completion of my project work.

I acknowledge the contribution of all other unseen hands during the course of the study for help rendered in successful completion of the study.

S.NANDHINI

Contents

CONTENTS

List of Tables

LIST OF TABLES

List of Figures

LIST OF FIGURES

List of Appendices

LIST OF APPENDICES

Introduction

1.0 INTRODUCTION

Earth's atmosphere was transformed from an anoxic state to the present fairly robust oxygen concentration of 20-21 per cent, after the formation of oceans, land and continents. The process by which Earth's atmosphere evolved from anoxic to oligoxic and oxic conditions continues to be a matter of debate and discussion, challenging many in this fascinating field of research. The increasing levels of atmospheric oxygen must have prompted anoxic life to an evolutionary race for survival. This race was won by oxic life and in stages, over at least 2 billion years, the evolution of plants and animals, including humans, created the world we live in today (Lindahl, 2008).

Photosynthetic organisms prospered and multiplied leading to a progressive increase of atmospheric O_2. O_2 related organelles, such as mitochondria, peroxisomes and plastids must have been acquired after that date (De Duve 2007; Semenza 2007). Peroxisomes may be responsible for as much as 20 percent of O_2 consumption and 35 percent of H_2O_2 production in tissues such as the liver (Schrader and Islinger, 2016).

In mammals, oxygen is extracted from the atmospheric air in the lungs, and carried by the bloodstream through the circulation to the tissue, where it is utilized mainly within the mitochondria. The human body is a complex living organism, which has developed mechanisms to keep oxygen levels in a suitable level to cover the metabolic demand, while avoiding excessive oxygen pressure (Prado *et al*., 2010). Oxygen (dioxygen, O_2) is mandatory to support human life from an early fetal stage onwards and for normal cellular function, as it is part of the electron transport chain for energy production in cells (Berner, 2007).

Oxygen plays an essential role in the respiratory process, the energy-producing chemistry that drives the metabolisms of most living things. Oxygen is essentially required by most eukaryotic organisms as a scavenger to remove harmful electron and hydrogen ions or as a critical substrate to ensure the proper execution of enzymatic reactions (Chen *et al.,* 2020). To maintain homeostasis, the amount of oxygen within the tissues should respond to a gradient of pressure that pushes oxygen by diffusion throughout the membranes into the tissues (Prado *et al*., 2010). Excess oxygen can be toxic to cells due to increased levels of damaging reactive oxygen species (Zenewicz, 2017).

Hypoxia is a state of low oxygen content and partial pressure in the cell. All nucleated cells can sense oxygen concentration and respond to reduced oxygen availability. When oxygen delivery is disrupted or reduced, the organisms will develop numerous adaptive mechanisms to facilitate cell survival in the hypoxic condition. Normally, such hypoxic response will cease when oxygen level is restored (Chen *et al.*, 2020).

Hypoxia, as one of the severe cellular stresses, can cause cellular injury and even cell death. Therefore, it is imperative to rescue or reverse acute hypoxia to prevent cell death in the event of acute hypoxia. Hypoxic conditions promote angiogenesis, glucose transport, anaerobic metabolism, invasion, resistance, and survival, particularly by modulating the apoptotic process (Al Tameemi *et al*., 2019). As a result of hypoxia, ATP levels drop, cellular functions cannot be maintained, and–if the insult lasts long enough– cells die. Oxygen depletion, which can lead to oxidative stress, nutrient deprivation and signaling disruption, can interfere with protein folding and subsequently, result in an accumulation of misfolded as well as unfolded proteins (Feldman *et al.,* 2005).

Sufficient delivery and perfusion of oxygen to the brain tissue are critical for avoiding life-threatening conditions. Acute hypoxia increases the formation of reactive oxygen species (ROS) in the brain. In acute hypoxia, cardiac output is increased to maintain systemic oxygen delivery and cerebral blood flow also increases to maintain oxygen delivery to the brain (Ando *et al.,* 2019*).* A classical example for an acute hypoxic event is stroke, caused by an occlusion of a brain artery (ischemia: restriction in blood supply) or hemorrhage. A stroke lesion can lead to both types of cell death, necrosis and apoptosis (Sendoel and Hengartner, 2014). Hypoxia potently induces the firing of carotid body nerves to stimulate ventilation and simultaneously cause vasoconstriction of pulmonary arteries (Sommer *et al.,* 2017).

Management of hypoxia falls under different categories: maintaining patient airways by ensure patency of the upper airways with good suctioning, maneuvers that prevent occlusion of the throat (head tilt and jaw thrust if necessary), sometimes the placement of an endotracheal tube or tracheostomy is necessary, increasing the percentage of oxygen in the inspired air that reaches the alveoli and improving the diffusion capacity. Nasal oxygen cannula is the most commonly used initial step for oxygen therapy in patients with mild hypoxia, due to its simplicity, reduced cost and ease of use. Reservoir Cannulas (Oxymizer) is the device that uses a

reservoir space, which stores oxygen during expiration, making it available as a bolus during the next inspiration. This way the patient gets a higher oxygen delivery without increasing flow (Bhutta *et al*., 2022).

High flow nasal cannula oxygen (HFNO) therapy is used increasingly in adults with acute respiratory failure before invasive ventilation, which delivers warm, humidified oxygen through the pliable nasal cannula with a fraction of inspired oxygen up to a maximum flow rate up to 70 L/min. Mild to moderate hypoxia is treated with nasal cannula oxygen. Severe hypoxia is treated by tracheal intubation and conventional mechanical ventilation (Jiang and Wei, 2020).

Nanotechnology has been a known field of research since last century. Since ‘‘nanotechnology” was presented by Nobel laureate Richard P. Feynman during his famous 1959 lecture ‘‘There’s Plenty of Room at the Bottom” (Feynman, 1960), various revolutionary developments have occurred in the field of nanotechnology. Nanotechnology produced materials of various types at nanoscale level. Nanoparticles (NPs) are a wide class of materials that include particulate substances, which have at least one dimension less than 100 nm (Laurent *et al*., 2010).

NPs are not simple molecules but are composed of three layers i.e. (a) The surface layer, which may be functionalized with a variety of small molecules, metal ions, surfactants and polymers. (b) The shell layer, which is chemically different material from the core in all aspects, and (c) The core, which is essentially the central portion of the NP and usually refers to the NP itself (Shin *et al*., 2016). NPs are broadly divided into various categories depending on their morphology, size and chemical properties. They are Carbon-based NPs, Metal NPs, Ceramics NPs, Semiconductor NPs, Polymeric NPs, Lipid-based NPs (Khan *et al.*, 2017).

Novel bionanotechnology employing engineered micro and nano structures has been developed for diagnostic and therapeutic applications in the field of healthcare. Nanovesicles, nanodroplets and nanobubbles have been examined as a substitute to readily available ultrasound contrast agents (Hadinger *et al*., 2018; Rojas and Dayton 2019; Nyankima *et al*., 2018; Dong *et al*., 2019; Xie *et al.,* 2018). Micro and nanobubbles are one of those new assemblies already in use in a variety of medical applications (Khan *et al*., 2019).

Nanometer size bubbles which are formed by insoluble gasses such as oxygen, nitrogen, carbon dioxide, hydrogen, helium etc., in liquid solutions and at solid–liquid interfaces are called nanobubbles. Nano shells can be prepared by using phospholipids, surfactants, polymers and proteins. The shell is a monolayer of a hydrophilic material that contains the core gas. The stability and biocompatibility of the nanobubbles depends on the type of the shells. It forms a protective layer around the gas to provide stability and protection from endogenous scavengers, and it reduces the rate of diffusion of the core gas into the surrounding media (Szabo, 2013).

Nanobubbles can migrate from vasculature to the extravascular target site, which greatly expands the application range of ultrasound molecular imaging. Similar to microbubbles, nanobubbles can also be used to load drugs or genes for therapy. Hence, nanobubbles have also been widely used in ultrasound molecular imaging and drug/gene targeting delivery. When conjugated with specific ligands, nanobubbles can be used as a probe in ultrasound molecular imaging of various diseases, such as tumor (Lv *et al*., 2018), allograft rejection (Liu *et al*., 2018), and so on. Because of their smaller size, nanobubbles can evade clearance by the reticuloendothelial system to a certain extent and have a longer retention time. Nanobubbles can promote more drug/gene aggregation and is non-cytotoxic (Rosen *et al*., 2012). Recently, nanobubbles have been investigated for theranostic (or theragnostic) applications, which involve combinations of diagnostic and therapeutic applications (Khan *et al*., 2019).

There are three types of nanobubbles: bulk nanobubbles, surface nanobubbles (also called "fine nanobubbles") and micro-pancakes (Zhang *et al.*, 2019). Bulk nanobubbles are described as gas-filled spherical bubbles found in liquid suspension that have a diameter less than 1000 nm, and are subjected to Brownian motion (Paknahad *et al*., 2021). The term surface nanobubbles is used to characterize gas-filled hemispherical caps that form on solid surfaces with a height within the range of 10–100 nm, and a radius within the range of 50–500 nm. Micro-pancakes which are quasi-two-dimensional gaseous domains, with lateral dimensions of several micrometers and a uniform height of a few nanometers (Nirmalkar *et al*., 2018).

Oxygen-filled bulk nanobubbles (either air or pure oxygen) can be used to enhance oxygen concentrations (Seddon *et al*., 2012). Oxygen nanobubbles are nanoscopic oxygen filled cavities in water. Oxygen nanobubbles have flexible structures with novel properties. (Bhandari *et al.,* 2017*).*

Oxygen nanobubbles (ONBs) are newly developed nanomaterials that can deliver oxygen to developing tissues and cells. ONBs have been used to successfully restore hypomineralized enamel and dentin caused by hypoxia by supplying oxygen (Kim *et al*., 2021).

The present study aims to assess whether these oxygen nanobubbles have the potential to reverse acute hypoxia in the isolated peripheral blood lymphocytes.

Review of Literature

2.0 REVIEW OF LITERATURE

The Review of Literature pertaining to the study entitled **"Assessing the ability of sodium carboxymethyl cellulose oxygen nanobubbles to reverse acute hypoxia in isolated peripheral blood lymphocytes"** is discussed under the following headings

2.1 Oxygen

2.1.1 Oxygen in atmosphere

Molecular oxygen (O_2) is arguably one of the most important elements on Earth, particularly for the aerobic organisms that depend on it to release energy from carbon-based macromolecules. The concentration of oxygen in the atmosphere is 20.95 percent (209,460 ppm) but this has fluctuated markedly throughout history. Earth is approximately 4.5 billion years old, and its early atmosphere contained virtually no oxygen whatsoever. The primitive atmosphere was instead formed mainly of hydrogen, with traces of methane and ammonia. Volcanoes then leached nitrogen and carbon dioxide into this mixture but it was not until the 'great oxygenation event,' approximately 2.3 billion years ago, that oxygen was released into the atmosphere by cyanobacteria that used carbon dioxide and sunlight to generate energy via photosynthesis (Lyons, 2014 and Holland, 2002).

As billions of years passed by, equilibrium was established whereby the concentration of oxygen fluctuated within a habitable range, between about 15 and 35 per cent, which has been maintained from the beginning of the Cambrian period 540 million years ago until the present day. Each surge in the atmosphere's oxygen concentration was accompanied by a new burst of life, while the troughs were associated with downscaling and extinction of species. The oscillation of the atmospheric oxygen concentration around a level that optimally promotes the development of multicellular organisms is termed the global oxygen cycle (Martin, 2017).

2.1.2 Oxygen in photosynthesis

The primary source of oxygen on Earth is photosynthesis, the generation of carbohydrates from carbon dioxide and water using sunlight as a catalyst (Eq. 1).

Photosynthesis:

$$6CO_2 + 6H_2O \rightarrow 6O_2 + C_6H_{12}O_6. \quad 1$$

Higher plants, algae, cyanobacteria and prochlorophytes are all capable of photosynthesis. A tiny amount of molecular oxygen is also produced by the photolysis of water vapor in the upper atmosphere (Eq. 2).

Photolysis:

$$2H_2O \rightarrow 4H^+ + e^- + O_2 \quad 2$$

The end-users of molecular oxygen are aerobic life forms, including humans, which use it to generate the majority of their energy requirements (Eq. 3).

Aerobic metabolism:

$$C_6H_{12}O_6 + 6O_2 \rightarrow 6CO_2 + 6H_2O \quad 3$$

As photosynthesizing cells spread across the planet, they eventually developed into complex multicellular plants. This crucial event in the developing ecosystem changed the world from a barely habitable rock into the luscious green environment that we recognize today. Over time, oxygen became the predominant mechanism for energy to be generated by non-photosynthesizing cells, through oxidative phosphorylation in mitochondria (Martin, 2017).

Oxygen is also used during photorespiration, in which organic substrates are oxidized to yield ATP for energetic processes, in some photosynthesizing cells (Matear and Hirst, 2003).

2.1.3 Oxygen in humans

A rise in the oxygen content of the atmosphere and oceans is one of the most popular explanations for the relatively late and abrupt appearance of animal life on Earth (Mills *et al*., 2014). Every time we take a breath in, oxygen is transported via the alveoli of the lungs to the capillaries and subsequently into the bloodstream. In the blood, hemoglobin, a protein in red blood cells (RBC), binds oxygen and shuttles it to tissues where the oxygen assists with nutrient breakdown and energy production. This process of delivering oxygen to tissues is known as perfusion (Meletis *et al.*, 2019).

Humans use oxygen to extract approximately 2550 Calories from food to meet daily energy requirements. This combustion requires about 22 moles of dioxygen per day, or 2.5×10^{-4} mol s^{-1}. This is an average rate of oxygen utilization of 2.5×10^{-18} mol $cell^{-1}$ s^{-1}, i.e. 2.5 amol $cell^{-1}$ s^{-1}. Cells have a wide range of oxygen utilization, depending on cell type, function, and biological status. Measured rates of oxygen utilization by mammalian cells in culture range from 350 amol $cell^{-1}$ s^{-1} (Wagner *et al.,* 2011).

2.2 Oxygen depletion

The atmosphere and sea act as the main reservoirs for oxygen and major events such as natural fires can alter the balance to a minor degree. Therefore, in simple terms, if the number of plants decreases, the oxygen-generating capacity of the Earth is reduced; and if the number of animals (including humans) increases, then oxygen consumption will rise. Combustion of fossil fuels has a major impact on oxygen and carbon dioxide levels in the atmosphere, there being a correlation between fossil fuel-related global warming and depletion of oxygen from the oceans (Matear and Hirst, 2003). Hypoxia is defined as oxygen deficiency in a biotic environment.

2.2.1 Hypoxia in atmosphere

Hypoxia can be caused by specific environmental conditions, which we refer to as "environmental hypoxia". Atmospheric hypoxia may result from either a decline in oxygen concentration (normobaric hypoxia) or a reduction in barometric pressure (hypobaric hypoxia) (Coppel *et al.,* 2015).

2.2.2 Hypoxia in aquatic environment

In aquatic environments, oxygen from the atmosphere or from phytoplankton dissolves in the water and helps to meet the respiration needs of all animals, including those that swim or move about the bottom and those that have a sedentary life. Once dissolved into surface waters, the normal condition is for dissolved oxygen to be mixed down into bottom waters. When the supply of oxygen to the bottom is cut off or the consumption rate exceeds resupply, oxygen concentrations decline beyond the point that sustains most animals. This condition of low dissolved oxygen is known as hypoxia (Diaz, 2001).

2.2.3 Hypoxia in plants

In plants, when the oxygen supply is insufficient, most cellular functions are compromised, which can lead to plant death (Loreti *et al.,* 2016). The term acute hypoxia is used when the drop in oxygen availability is transitory in plants, which can be due to adverse environmental conditions such as flooding events or when unusual, transient increases in oxygen consumption occur in a plant tissue. Acute hypoxia is perceived by the plants as stressful. On the other hand, chronic hypoxia is a constitutive and usually non-stressful condition where the oxygen level is maintained low only in a given group of cells and not in the entire plant. In other words, chronic hypoxia can be a physiological condition in specific plant tissues (Weits *et al.,* 2021).

2.2.4 Hypoxia in humans

In humans, a hypoxic state indicates that an imbalance of oxygen is present and baseline function is compromised as a result of this imbalance. The imbalance of oxygen could result from a lack of oxygen or an excessive demand for oxygen. Baseline function in this context means carrying out normal bodily or cellular functions such as heart muscle beating or a neuron firing an action potential, also known as homeostasis. Hypoxia can be transient, acute or chronic. Hypoxic conditions occur with a persistent lack of oxygen. Individual tissues have differing oxygen tensions and oxygen demands; on average, tissues at rest utilize 5–6 mL of O_2 per deciliter of blood delivered. Hypoxia could be fairly defined as a scenario when tissue fails to receive this amount of oxygen (Choudhury *et al.*, 2018).

2.2.5 Causes of hypoxia

Hypoxia results in pain and suboptimal cellular function. Tight muscles are reflective of a hypoxic state (Meletis *et al.,* 2019). A lack of oxygen can be due to environmental hypoxia at high altitudes, where the partial oxygen pressure (pO_2) is decreased in proportion to the lower ambient pressure (Burtscher *et al.,* 2018). Besides environmental hypoxia, pathological conditions such as chronic obstructive pulmonary disease (Baldi *et al.,* 2010), obstructive sleep apnea (Garvey *et al.,* 2009) and anemia (Grocott *et al.,* 2007) can also lead to hypoxia.

Hypoxia can arise as a consequence of impaired blood flow. This can significantly damage organ structure and function, resulting, for example, in a stroke (cerebral ischemia) or heart infarction (myocardial ischemia). Hypoxia also regulates tumor growth and metastasis (Michiels, 2004).

2.2.6 Types of hypoxia

Hypoxia is actually divided into four types as follows:

2.2.6.1 Hypoxemic Hypoxia

Hypoxemic Hypoxia is defined as Low oxygen tension in the arterial blood (PaO2) is due to the inability of the lungs to properly oxygenate the blood. Causes include hypoventilation, impaired alveolar diffusion, and pulmonary shunting**.**

2.2.6.2 Circulatory Hypoxia

Circulatory Hypoxia is due to pump failure (heart is unable to pump enough blood, and therefore oxygen delivery is impaired).

2.2.6.3 Anemic Hypoxia

Anemic Hypoxia is because of a decrease in oxygen-carrying capacity due to low hemoglobin leading to inadequate oxygen delivery.

2.2.6.4 Histotoxic Hypoxia (Dysoxia)

In dysoxia, cells are unable to utilize oxygen effectively (Bhutta, *et al.,* 2021).

2.2.7 Adaptation to hypoxia

Humans have the ability to adapt to hypoxemia, through a process known as acclimatization, but the extent to which adaptation can compensate for the oxygen deficit depends on the magnitude of the deficit and the time over which it occurs (Martin *et al.*, 2016).

2.2.7.1 Adaptation to acute hypoxia

A significant and abrupt fall in partial pressure cannot be tolerated for more than a few minutes since cerebral hypoxia results in unconsciousness. Descriptions of death following sudden oxygen deprivation were common amongst early high-altitude aviators during World War II (Martin *et al.*, 2016).

2.2.7.2 Adaptation to subacute hypoxia

With a more gradual exposure to hypoxia, as might be experienced during a trek to high altitude, other biological systems have a chance to adapt through a process known as acclimatization. Hypoxia is sensed at a cellular level, triggering the increased concentration of a gene regulator known as hypoxia inducible factor (HIF). One important role of HIF is to increase the number of circulating red blood cells through the up-regulation of erythropoietin. This

increases the oxygen-carrying capacity of the blood over a period of days to weeks and forms the backbone of short-term hypoxic adaptation(Martin *et al.*, 2016).

2.2.7.3 Lifelong hypoxic exposure

Chronic disease or long-term residence at high altitude can expose humans to a lifetime of hypoxemia. With increasing altitude of residence, chronic mountain sickness (CMS) and intrauterine growth retardation (IUGR) become more prevalent. CMS is characterized by excessive polycythemia, progressing to pulmonary hypertension, right ventricular failure and death (Martin *et al.*, 2016).

2.2.8 Hypoxia and human diseases

2.2.8.1 Cancer

Impaired oxygen delivery and consumption are typical features of hypoxia in tumor microenvironment. The rise of hypoxia first comes from the restriction of oxygen diffusion in avascular primary tumors along with the higher oxygen consumption due to hyperproliferation of cancer cells. Cellular responses to hypoxia are essential for tumor progression in many aspects, such as cancer cell survival, proliferation, epithelial-to-mesenchymal transition (EMT), invasion, angiogenesis, drug resistance, and metastasis (Schito, *et al.*, 2016).

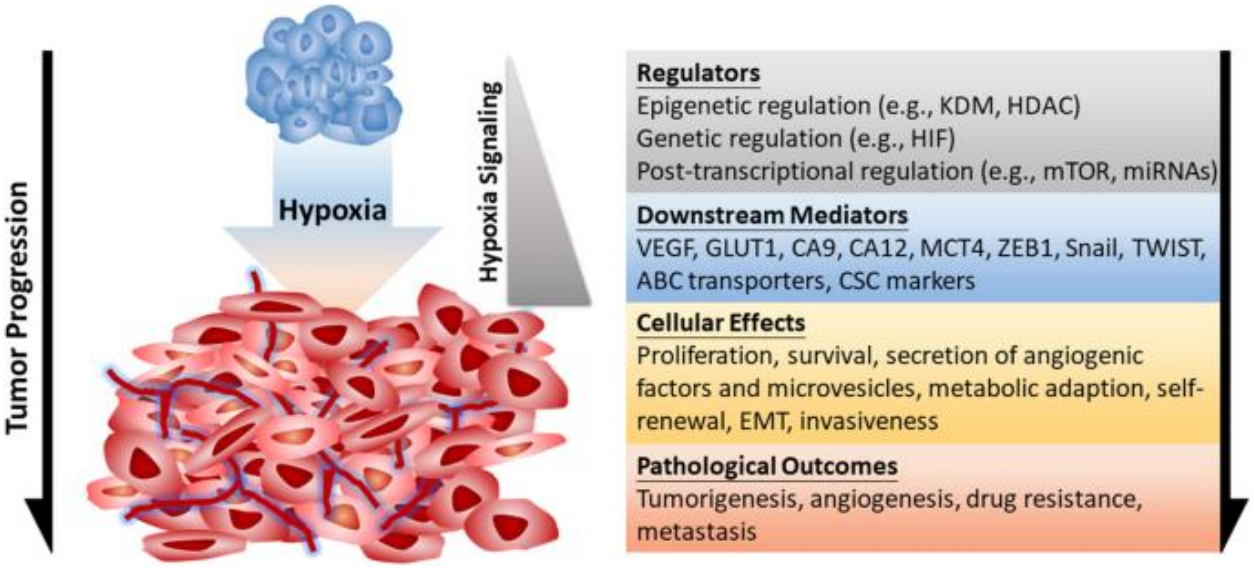

Figure 1

Hypoxia-regulated cancer progression (Chen *et al.*, 2020).

Hypoxia is a typical feature of tumor microenvironment, which contributes to initial tumorigenesis, induced angiogenesis, drug resistance, and cancer metastasis. The major upstream regulators (gray), functional downstream genes (blue) and resulting cellular consequences (yellow) under the control of hypoxia signaling are indicated in Figure 1 (Chen *et al.,* 2020).

2.2.8.2 Cardiovascular diseases

Heart failure with reduced left ventricular systolic function after myocardial infarction causes insufficient oxygen in the body leading to systemic and pulmonary hypertension. Atherosclerosis is a chronic inflammatory disease that can increase the risk of myocardial infarction and stroke. The thickness of arterial wall causes hypoxia in the intima, reduces the perfusion of the tissue, and further stimulates proatherosclerotic processes, like inflammation, lipid synthesis and angiogenesis (Sluimer *et al.,* 2009)

2.2.8.3 Altered metabolism

Hypoxia is one of the mechanisms responsible for the development of metabolic changes and pro-inflammatory situations of white adipose tissue. In obesity, due to the enlargement of adipocytes and increased distance from the vasculature, hypoxia occurs within the expanding white adipose tissue (Trayhurn *et al.,* 2008) and alters several key metabolic processes including glucose uptake, glycolysis, oxidative metabolism, lipolysis and lipogenesis (Rocha, 2007). Hypoxia triggers reactive oxygen species (ROS) production, endoplasmic reticulum stress, inflammatory responses, angiogenesis and adipocyte death (Koumenis *et al.,* 2002).

2.2.8.4 Kidney diseases

Loss of microvasculature, reduced oxygen dispersion, and metabolic abnormality of cells in the kidney are the main causes of the hypoxic state (LeBleu *et al.,* 2013). Hypoxia leads to renal fibrosis and functional loss of kidney (Lovisa *et al.,* 2016).

Figure 2

Schematic diagram of the hypoxic process linked to kidney diseases

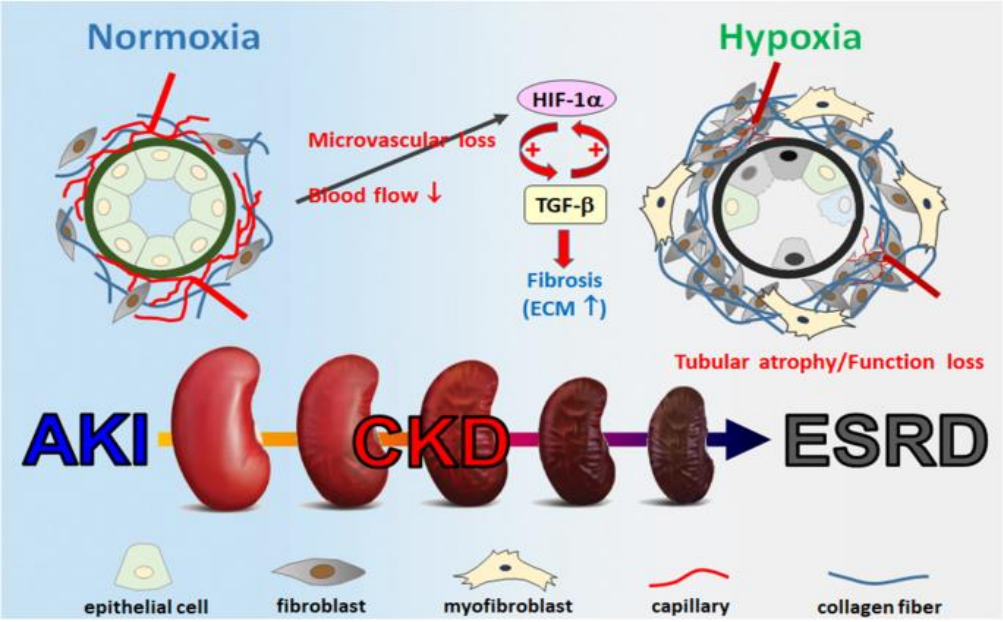

Adapted from Chen *et al.* (2020)

During the development of chronic kidney disease (CKD), vascular endothelial cells die and cause atrophy of microvessels. This will cause local hypoxia between tissues and cause inflammatory reactions. Hypoxia induces the expression of transforming growth factor-β, which leads to fibroblast transformation into myofibroblast, increases extracellular matrix production and causes fibrosis. Renal tubular epithelial cells may encounter cell cycle arrest, apoptosis, autophagy and finally shrink during renal fibrosis. These data indicate that hypoxia and HIF-1α have a pivotal role in mediating kidney fibrosis (Chen *et al.,* 2020) as shown in Figure 2.

2.2.8.5 Cerebral hypoxia

Cerebral hypoxia and subsequent reoxygenation is a central component of several diseases, such as traumatic brain injury, acute respiratory distress syndrome, obstructive sleep apnea, high-altitude cerebral edema and acute mountain sickness, cardiac arrest, and ischemic stroke. As a result of hypoxia, ATP levels drop, cellular functions cannot be maintained, and–if the insult lasts long enough–cells die (Sendoel and Hengartner, 2014). Hypoxia can be managed by maintaining patency airways, increasing the oxygen content of the inspired air, improving the diffusion capacity, simple face mask,etc (Bhutta *et al.*, 2022).

2.2.9 Treatment methods for hypoxia

The most common reasons for initiating oxygen therapy include acute hypoxemia related to pneumonia, shock, asthma, heart failure, pulmonary embolism, myocardial infarction resulting

in hypoxemia, post operative states, pneumothorax, and abnormalities in the quality and quantity of hemoglobin. Raising the head of the bed promotes effective breathing and diaphragmatic descent, maximizes inhalation and decreases the work of breathing. Positioning enhances airway patency in all hypoxic people. Deep breathing and coughing techniques help patients effectively clear their airway while maintaining their oxygen levels. Hyperbaric oxygen therapy is a treatment for hypoxic- and inflammatory-driven conditions, in which patients are treated with 100% oxygen at pressures greater than atmospheric pressure (Kane *et al.*, 2013).

2.2.9.1 Hyperbaric oxygen therapy (HBOT)

Using Dalton's and Henry's laws, we can see that the physiologic effect of Hyperbaric oxygen therapy alters the concentration of oxygen in the plasma and assists hemoglobin to achieve full oxygen-carrying capacity. HBOT is the use of oxygen under pressure "as a drug to treat basic disease processes and their diseases". The effects of hyperbaric oxygen lead to changes in the transcription of DNA, alterations in the organelles of the cell, improved structure of tissue and more efficient function of the organ. These changes can become permanent within 25–35 treatments. Hyperbaric oxygen was first used in 1937 by Behnke and Shaw to treat decompression sickness. After the success of Behnke and Shaw, multiple uses for HBOT were explored. A year later in 1938, Ozorio de Almeida and Costa treated patients suffering from leprosy with HBOT. By 1960, Sharp and Smith treated cases of carbon monoxide poisoning using HBOT. In 1961, Boerema and Brummelkamp used HBOT for gas gangrene. Perrins demonstrated the use of HBOT for osteomyelitis in 1965. Then in 1983, the American College of Hyperbaric Medicine was founded by Dr Neubauer. During this time, the safety features and designs of hyperbaric chambers improved as the indications for therapy expanded (Choudhury *et al*., 2018).

HBOT is currently administered in chambers of varying sizes ranging from personal units to surgical operating rooms every day. HBOT has many current indications for treatment due to its ability to counter oxygen deficits, promote healing and angiogenesis, fight infection and control inflammation (Choudhury *et al.*, 2018).

2.3 Nanotechnology

Nanotechnology is an excellent example of an emerging technology, offering engineered nanomaterials with the great potential for producing products with substantially improved performances (Marques *et al.*, 2021). It is expected that nanotechnology will be developed at several levels: materials, devices and systems. The nanomaterial level is the most advanced at present, both in scientific knowledge and in commercial applications (Salata, 2004).

A description of various terms associated with nanomaterials are as follows: (Baig *et al.*, 2021)

Term	**Description**
Nanotechnology	Nanotechnology refers to technology at the nanoscale level in which materials, devices, or systems are developed via controlling matter at the nanoscale length to stimulate the unique properties of the material at the nano-level.
Nanomanufacturing	Nanomanufacturing refers to manufacturing at the nanoscale level and accomplished *via* bottom-up or top-down methods.
Nanoscale	A scale covering 1–100 nm.
Nanomaterial	A material is called a nanomaterial if it has at least one dimension in the nanoscale range of 1–100 nm.
Nano-object	A nano-object is a discrete piece of material with one, two, or three external dimensions in the nanoscale range.
Nanoparticle	An object or particle is called a nanoparticle when all of its dimensions are in the nanoscale range.
Aspect ratio	The aspect ratio of a nano-object is defined as the ratio of the length of the major axis to the width of the minor axis.
Nanosphere	A nanosphere is a nanoparticle that has an aspect ratio of 1.
Nanorod	The term nanorod is used when the shortest and longest axes have different lengths. Nanorods have a width in the range of 1 to 100 nm and an aspect ratio greater than 1.
Nanofiber	A nano-object with two dimensions in the nanoscale range and a third

Term	Description
	dimension that is significantly larger.
Nanowire	Nanowires are analogues to nanorods, but with a higher aspect ratio.
Nanotube	Hollow nanofibers are called nanotubes.
Nanostructured material	This is a term used for materials that have structural elements, molecules, crystallites, or clusters with dimensions in the range of 1–100 nm.
Nanomaterial	A material is called a nanomaterial if it has at least one dimension in the nanoscale range of 1–100 nm.
Engineered nanomaterials	Intentionally produced materials that have one or more dimensions in the order of 100 nm or less are called engineered nanomaterials.
Nanocomposite	Nanocomposites are defined as multicomponent materials with multiple different phase domains, in which at least one of the phases has at least one dimension in the order of nanometers.

2.3.1 Nanomaterials

A nanometer (nm) is an International System of Units (Système international d'unités, SI) unit that represents 10^{-9} meter in length. In principle, nanomaterials are described as materials with length of 1–1000 nm in at least one dimension; however, they are commonly defined to be of diameter in the range of 1 to 100 nm (Boverhof *et al.*, 2015).

2.3.2 Application of nanomaterials

Figure 3

Schematic representation of nanomaterials and their applications (Baig *et al.*, 2021)

Synthesis methods, properties, and possible opportunities relating to the broad and fascinating area of nanomaterials are shown in Figure 3. There are several important applications of nanomaterials such as aviation and space, chemical industry, optics, solar hydrogen, fuel cell, batteries, sensors, power generation, aeronautic industry, building/construction industry, automotive engineering, consumer electronics, thermoelectric devices, pharmaceuticals and cosmetic industry (Salata 2004).

2.3.2.1 Biology and medicine

A list of some of the applications of nanomaterials to biology or medicine are Fluorescent biological labels, drug and gene delivery, bio detection of pathogens, detection of proteins, probing of DNA structure, tissue engineering, tumor destruction via heating (hyperthermia),

separation and purification of biological molecules and cells, MRI contrast enhancement, pharmacokinetic studies etc,. (Salata 2004).

2.3.2.2 Agriculture and food industries

Nanomaterials can be utilized in the agri food industries as nanoformulations for crop improvement, in crop protection for the identification of diseases, nanodevices for the genetic manipulation of plants, plant disease diagnostics, etc. A number of nanoparticles (mostly metal-based and carbon-based nanomaterials) have been exploited to improve the growth and development of crop food plants (Agrawal and Rathore, 2014). This positive impact has led to enhanced germination percentage, biomass production along with enhancement of physiological parameters such as photosynthesis and nitrogen metabolism in many food crops including alfalfa, cucumber, corn, lettuce, onion, pumpkin, ryegrass, rape, radish, spinach, soybean, tomato, and wheat (Nair *et al.,* 2010).

Nanomaterial has given a promise in plant protection, via genetically modified crops to produce a plant disease resistance to pathogen infections and is crucial to ensure sustainable food and agriculture. Nanoencapsulation displays the advantage of more efficient use and safer handling of pesticides, fertilizers and vaccines with less exposure to the environment that guarantees eco-protection. Nanofertilizers have unique features like ultrahigh absorption which is a route to enrich the soil with adequate essential nutrients gradually, thus preventing pollution of water resources and it is well known to improve the quantity of fruit and biological production Nanotechnology can play a role in the detection of pathogens or pesticides in food. They can also monitor the temperature and pH of foods to prevent the presence of these unwanted organisms through the use of nanosensors (Naderi and Shahraki, 2013).

Currently, nanomaterials find commercial roles in scratch-free paints, surface coatings, electronics, cosmetics, environmental remediation, sports equipment, sensors, and energy-storage devices (Baig *et al.,* 2021)

2.3.3 Nanoparticles

Nanoparticles are a particular type of nanomaterial that can occur naturally, be created unintentionally, or indeed be engineered on purpose (Prajitha *et al.,* 2019). Nanoparticles (NPs) are wide class of materials that include particulate substances, which have one dimension less than 100 nm at least (Laurent *et al*., 2010).

2.3.3.1 Nanoparticle composition

NPs are not simple molecules itself and therefore composed of three layers i.e. (a) The surface layer, which may be functionalized with a variety of small molecules, metal ions, surfactants and polymers (b) The shell layer, which is chemically different material from the core in all aspects, and (c) The core, which is essentially the central portion of the NP and usually refers to the NP itself (Shin *et al*., 2016).

2.3.3.2 Classification of nanoparticles

NPs are broadly divided into various categories depending on their morphology, size and chemical properties. They are Carbon-based NPs, Metal NPs, Ceramics NPs, Semiconductor NPs, Polymeric NPs and Lipid-based NPs (Khan *et al.*, 2019).

Carbon-based NPs

Fullerenes and carbon nanotubes (CNTs) represent two major classes of carbon-based NPs. Fullerenes contain nanomaterial that are made of globular hollow cage such as allotropic forms of carbon. They have created noteworthy commercial interest due to their electrical conductivity, high strength, structure, electron affinity, and versatility (Astefanei *et al*., 2015).

Metal NPs

Metal NPs are purely made of the metals precursors. Due to well-known localized surface plasmon resonance characteristics, these NPs possess unique optoelectrical properties. NPs of the alkali and noble metals i.e. Cu, Ag and Au have a broad absorption band in the visible zone of the electromagnetic solar spectrum. The facet, size and shape controlled synthesis of metal NPs is important in present day cutting-edge materials (Dreaden *et al*., 2012).

Ceramics NPs

Ceramics NPs are inorganic nonmetallic solids, synthesized via heat and successive cooling. They can be found in amorphous, polycrystalline, dense, porous or hollow forms (Sigmund *et al*., 2006). Therefore, these NPs are getting great attention of researchers due to their use in applications such as catalysis, photocatalysis, photodegradation of dyes and imaging applications (Thomas *et al*., 2015). Semiconductor materials possess properties between metals and nonmetals and therefore they found various applications in the literature due to this property (Ali *et al*., 2017, Khan *et al*., 2017). Semiconductor NPs possess wide bandgaps and therefore showed significant alteration in their properties with bandgap tuning. Therefore, they are important materials in photocatalysis, photo optics and electronic devices (Sun, 2000).

Polymeric NPs

These are normally organic based NPs and in the literature a special term polymer nanoparticle (PNP) collective is used for it. They are mostly nanospheres or nano capsular shaped (Mansha *et al*., 2017). The former are matrix particles whose overall mass is generally solid and the other molecules are adsorbed at the outer boundary of the spherical surface. In the latter case the solid mass is encapsulated within the particle completely (Rao and Geckeler, 2011).

Lipid-based NPs

These NPs contain lipid moieties and are effectively used in many biomedical applications. Generally, a lipid NP is characteristically spherical with diameter ranging from 10 to 1000 nm. Like polymeric NPs, lipid NPs possess a solid core made of lipid and a matrix contains soluble lipophilic molecules. Surfactants or emulsifiers stabilized the external core of these NPs (Rawat *et al.,* 2011). Lipid nanotechnology (Mashaghi *et al.,* 2013) is a special field, which focus the designing and synthesis of lipid NPs for various applications such as drug carriers and delivery (Puri *et al.,* 2009) and RNA release in cancer therapy (Gujrati *et al.,* 2014).

2.3.3.3. Applications of Nanoparticles

Gold nanoparticles are widely used in immunohistochemistry to identify protein-protein interaction. Colloidal silver is widely used in anti-microbial formulations and dressings. The high reactivity of titania nanoparticles, either on their own or then illuminated with UV light, is also used for bactericidal purposes in filters. Enhanced catalytic properties of surfaces of nano-ceramics or those of noble metals like platinum are used to destruct dangerous toxins and other hazardous organic materials (Salata, 2004).

2.4 Nanobubbles

Novel bionanotechnology employing engineered micro and nano structures has been developed for diagnostic and therapeutic applications in the field of healthcare (Choi *et al.,* 2015). Micro and nanobubbles are one of those new assemblies already in use in a variety of medical applications, typically as ultrasound contrast agents (Cavalli *et al.,* 2013). Recently,

nanobubbles have been investigated for theranostic (or theragnostic) applications, which involve combinations of diagnostic and therapeutic applications. Nanobubbles mostly consist of similar shell/core compositions, in which the shell is often formed of a unilaminar composition of phospholipids, polymers, or proteins and the core contains a less soluble gas (Khan *et al*., 2018). Nanobubbles are of particular interest, owing to their smaller size, biodegradability, higher surface area, longer half-life, higher cellular uptake and echogenic properties (Cavalli *et al.*, 2016).

2.4.1 Types of nanobubbles

There are three types of nanobubbles: bulk nanobubbles, surface nanobubbles (also called "fine nanobubbles") and micro-pancakes (Zhang *et al.*, 2019). The term surface nanobubbles is used to characterize gas-filled hemispherical caps that form on solid surfaces with a height within the range of 10–100 nm, and a radius within the range of 50–500 nm. Bulk nanobubbles are described as gas-filled spherical bubbles found in liquid suspension that have a diameter less than 1000 nm, and are subjected to Brownian motion (Paknahad *et al*., 2021). Micro-pancakes which are quasi-two-dimensional gaseous domains, with lateral dimensions of several micrometers and a uniform height of a few nanometers (Nirmalkar *et al*., 2018).

2.4.2 Composition of nanobubbles

Nanometer size bubbles which are formed by insoluble gasses such as oxygen, nitrogen, carbon dioxide, hydrogen, helium etc., in liquid solutions and at solid–liquid interfaces are called nanobubbles. Nano shell can be prepared by using phospholipids, surfactants, polymers and proteins. The shell is a monolayer of a hydrophilic material that contains the core gas. The stability and biocompatibility of the nanobubbles depends on the type of the shells. It forms a protective layer around the gas to provide stability and protection from endogenous scavengers, it reduces the rate of diffusion of the core gas into the surrounding media (Szabo, 2013).

2.4.3 Methods to synthesis nanobubbles (NBs)

NBs are synthesized by various methods such as sonication, Ink-Jet method, microfluidic techniques, laser ablation method, agitation method and emulsification method.

2.4.3.1 Sonication

Sonication is a popular method to synthesize micro/nanobubbles (MNBs) in a single step. This method is applied to synthesize MNBs of various types of shell coatings including lipids,

polymers, proteins and surfactants. When ultrasound is applied in a medium, the compressions and rarefactions produce high-pressure and low-pressure zones in the fluid. In addition, if there are surfactants or coating materials present in the medium, the ultrasonic pressure may destroy them, thereby causing them to take new forms, thus stabilizing the gas–liquid interface by the formation of MNBs (Cavalli *et al*., 2016).

The process of cavitation and bubble formation is not fully understood. Sonication is a stochastic method and therefore, generates MNBs of random sizes. However, the size distribution can be controlled using sonication parameters, such as frequency, pulse duration, and power (McEwan *et al*., 2015 and Khan *et al.,* 2018)

Commercial sonicators like bath-tub and tip sonicators are also available for synthesizing MNBs. The limitation of the sonication method is the productivity and yield of the MNBs. This is because only a limited amount of solutions can be sonicated within a given time. Therefore, researchers have investigated other methods for a high yield (Kheir *et al.,* 2013).

2.4.3.2 Ink-Jet Method

Microbubble synthesis has been performed using an ink-jet method, in which a polymer solution is forced through a piezo-driven ink-jet nozzle of a desirable size, depending on the application. The piezoelectric crystals create pulses in the solution and the bubbles that are formed are removed from the nozzle. A similar method has also been applied to generate ultrafine oxygen nanobubbles from pure water and an oxygen supply by utilizing a high-pressure flow through the nozzle (Iijima *et al*., 2018).

2.4.3.3 Microfluidic Techniques

Microfluidic devices have the ability to synthesize MNBs with controlled size distributions. Flow rate, pressure, viscosity of the liquid solution, and the orifice size of the device can be controlled to determine the size and distribution of the MNBs. To the two main methods for the fabrication of microfluidic devices are as follows:

(1) Soft lithography techniques to produce flow focusing units

(2) mechanically assembled units from capillaries assembled in a polymeric block.

The gas and liquid flows into a T-junction in both cases The MNBs are then generated in the T-junction depending on the size of orifice and other parameters of the device being used.

2.4.3.4. Laser Ablation Method

The laser ablation method is also a stochastic method that can generate MNBs. An excimer laser of a particular wavelength can be focused onto aluminum oxide particles in water, which then forms oxidized nanoparticles. During the process, bubbles will also be produced at the solid–liquid interface. The bubbles/interfaces are stabilized by the aluminum oxide nanoclusters (Lee *et al*., 2015).

2.4.3.5. Agitation Method

MNBs, especially those having lipid shells, can be produced by agitating the liquid solution at several thousand oscillations per minute in a shaker. This will produce bubbles with a random size distribution. To encapsulate a given gas in an MNB, the container is filled with the desired coating material in the liquid phase and the gas is perfused from the top and then the container is mechanically agitated so that the shell material encapsulates the desired gas (Sun *et al*., 2016). Mechanical agitation is a promising method to produce MNBs on an industrial scale.

2.4.3.6 Emulsification Method

This method is usually applied to synthesize polymer shell MNBs. In this process, water is formed in an oil emulsion with a carrier polymer, and this emulsion is further emulsified in a large volume of water. The solvent is evaporated or extracted to obtain a solid polymer shell, and lyophilized shells are refilled with core gas, such as perfluorocarbon (PFC) (Xu *et al.,* 2011). A high-shear emulsification method has been used to synthesize MNBs with a broader size range. A membrane emulsification method can be used to generate MNBs with a narrow size distribution. A porous membrane is used for this purpose. Gas bubbles permeate and disperse into a continuous phase flowing along the membrane surface. Emulsifiers are added to prevent coalescence.

2.4.4 Application of nanobubbles

Nanobubbles have been widely used in ultrasound molecular imaging and drug/gene targeting delivery. When conjugated with specific ligands, nanobubbles can be used as a probe in ultrasound molecular imaging of various diseases, such as tumor (Lv *et al*., 2018), allograft rejection (Liu *et al*., 2018), and so on.

Nanobubbles can migrate from vasculature to the extravascular target site, which greatly expands the application range of ultrasound molecular imaging. Nanobubbles can also be used to load drugs or genes for therapy. Because of their smaller size, nanobubbles can evade clearance

by the reticuloendothelial system to a certain extent and have a longer retention time. Nanobubbles can promote more drug/gene aggregation and is non-cytotoxic (Rosen *et al*., 2012).

In the work of US imaging, bubbles were also attaining considerable interest from the investigators other than drug delivery. Recently, nanobubbles are produced as drug vectors or contrast agents predominantly for cancer associated molecular imaging through the size effects (Zhang *et al*., 2019).

2.4.5 Oxygen nanobubbles

Oxygen nanobubbles (ONBs) are newly developed nanomaterials that can deliver oxygen to developing tissues and cells. Nanobubbles can be utilized to create supersaturated fluids for oxygen delivery (Khan *et al.,* 2019). Oxygen-filled nanobubbles (oxygen nanobubbles) have potential applications in various fields: nanofluidics (Wang et al., 2011), nanochemistry (Rettew *et al.,* 2011) nanomechanics, nanomedicine and environmental treatment because of their ability to produce free radicals.

Oxygen nanobubbles have also been employed for detoxification of water and degradation of organic compounds in wastewater treatment (Wang *et al*., 2009). Moreover, oxygen nanobubbles loaded on porous solid particles of natural clay can be purposely delivered to eutrophic shallow lakes or anoxic sediment and efficiently revive polluted lakes (Zhang *et al*., 2018). ONB can be used to successfully restore hypomineralized enamel and dentin caused by hypoxia by supplying oxygen (Kim *et al.,* 2021). Oxygen-containing microbubbles/nanobubbles have been developed to supply oxygen and enhance the effects of therapies such as radiotherapy and photodynamic therapy (Puri *et al.,* 2009).

Our aim is to synthesize oxygen nanobubbles by ultrasonication, characterize to determine morphology, surface area, dissolved oxygen content, elemental analysis and structure. We then propose to assess its ability to reverse acute hypoxia in peripheral blood lymphocytes.

Methodology

3.0 METHODOLOGY

Oxygen (dioxygen, O_2) is mandatory to support human life from an early fetal stage onwards and for normal cellular function, as it is part of the electron transport chain for energy production in cells (Berner, 2007).

Hypoxia, as one of the severe cellular stresses, can cause cellular injury and even cell death. Therefore, it is imperative to rescue or reverse acute hypoxia to prevent cell death in the event of acute hypoxemia and hypoxia (Al Tameemi *et al*., 2019).

Lymphocytes are good model cells to study cellular responses. Hence, the present study was designed to investigate the therapeutic potential of oxygen nanobubbles to deliver oxygen to lymphocytes exposed to the hypoxic agent cobalt chloride.

The methodology pertaining to the study entitled **"Assessing the ability of sodium carboxymethyl cellulose oxygen nanobubbles to reverse acute hypoxia in isolated peripheral blood lymphocytes"** is discussed under the following headings:

3.1 Synthesis of sodium carboxy methyl cellulose oxygen nanobubbles (SCMC- ONB)

3.2 Characterization of oxygen nanobubbles

3.2.1 Field Emission Scanning Electron Microscope (FESEM)

3.2.2 Energy-dispersive X-ray spectroscopy (EDX)

3.2.3 Fourier Transform Infrared Spectroscopy (FTIR)

3.2.4 3 Dimensional Optical profiler (3D Optical profiler)

3.2.5 X-ray Diffraction (XRD)

3.2.6 Dissolved oxygen content

3.3 Assessment of hypoxia reversal

3.3.1 Ethical Approval

3.3.2 Sample collection

3.3.3 Isolation of Lymphocytes

3.3.4 Induction of Hypoxia using Cobalt Chloride

3.3.5 Cell viability: Trypan blue assay

3.3.6 Assessment of Hypoxia Reversal by SCMC-ONB Treatment

3.3.7 Statistical analysis

Work plan

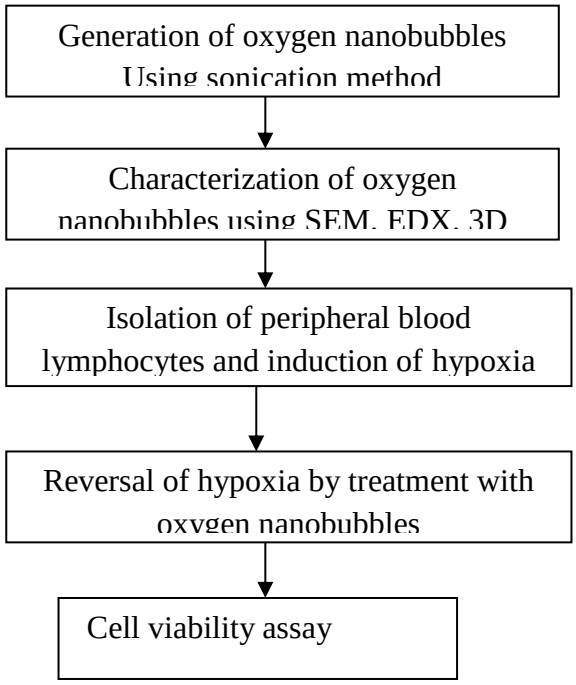

3.1 Synthesis of sodium carboxy methyl cellulose oxygen nanobubbles (SCMC- ONB)

There are various techniques used to synthesize nanobubbles such as sonication, ink-jet method, microfluidic method, laser ablation method, agitation method and emulsification method (Szabo, 2013). Sonication is a stochastic method and, therefore, generates nanobubbles of random sizes. However, the size distribution can be controlled using sonication parameters, such as frequency, pulse duration, and power (Stride *et al.,* 2008). Sodium carboxymethyl cellulose acts as a polymer shell for oxygen nanobubble production (Bhandari *et al.* 2017). Therefore, in the present study, nanobubbles were synthesized by sonication method following the protocol by

Bhandari *et al.* (2017) as shown in Appendix I. Synthesis of SCMC-ONB was tried three different times with different parameters as shown in Table 1.

Table 1

Synthesis of SCMC-ONB

S.No	Samples	Duration of sonication (minutes)	Temperature (°C)	Frequency (kHz)	Power (Watts)	Oxygen infusion time (minutes)
1.	SCMC-ONB 1	60	40	40	70	60
2.	SCMC-ONB 2	120	40	40	70	120
3.	SCMC-ONB 3	5	37	20	130	20

3.2 Characterization of oxygen nanobubbles

The synthesized catalysts were characterized by FESEM, EDX, FTIR,3D Optical profiler, XRD, Dissolved oxygen content.

3.2.1 Field Emission Scanning Electron Microscope (FESEM)

FESEM produces clearer, less electrostatically distorted images with spatial resolution down to 1 1/2 nanometers Mayeen *et al*., (2018). The surface morphology of the SCMC- ONB was investigated by performing a Field Emission Scanning Electron Microscopy (SEM) analysis using a Quanta 250 FEG following the protocol by Chung *et al*. (2017) described in Appendix II.

3.2.2 Energy Dispersive X-Ray Analysis (EDX)

EDX is used to determine the composition of a sample such as thin films. Not only can relative amounts of each atom be measured, but the distribution of the atoms in our samples can

be mapped (https://www.cei.washington.edu). It can be used for both qualitative and quantitative analysis. SCMC- ONB were analyzed for elemental composition using QUANTAX EDS SOP BRUKER following the procedure by Chung *et al*. (2017) detailed in Appendix III.

3.2.3 Fourier Transform Infrared Spectroscopy (FTIR)

FTIR is a universal analytical tool for evaluation of a wide range of materials, especially for identification of unknown materials. It has been used to identify pure substances, mixtures, impurities and compositions of various materials Kowalczuk and Pitucha, (2019). FTIR-SHIMADZU (Miracle10) were used to identify the presence of functional groups in SCMC-ONB following the protocol by Fadlelmoula *et al*. (2022) as shown in Appendix IV.

3.2.4 3D Optical profiler

3D Optical profiler is to enable precise, quantitative, non-contact surface measurement and characterization of micro- and nano-scale surface features, capturing up to two million data points in just seconds. It is used to measure height variations such as surface roughness on surfaces, with great precision, using the wavelength of light as the ruler (https://www.e-education.psu.edu/mcl-optpro/theory/node789). In order to investigate the surface area and roughness of SCMC-ONB, analysis was carried out using an LASER PROFILOMETER - Zeta-20 by following the protocol by Kapłonek *et al.* (2020) as shown in Appendix V.

3.2.5 X-ray diffraction (XRD)

XRD is a rapid and powerful technique that helps to find the geometry or shape of a molecule using X-rays and to identify unknown minerals and materials (https://www.scimed.co.uk/education/what-is-x-ray-diffraction-xrd/). It only requires preparation of a minimal sample for analysis. Interpreting the resulting data is relatively straightforward. PANalytical X'Pert Pro was used to identify the crystalline structure of SCMC-ONB, following the protocol by Miatmoko *et al*. (2021) as shown in Appendix VI.

3.2.6 Dissolved Oxygen Content

Dissolved oxygen meters are designed to measure the amount of gaseous oxygen dissolved in samples. They also help to evaluate sample quality (Wei, 2019). Dissolved oxygen content in SCMC- ONB was measured by an electrochemical DO sensor, following the protocol by Hu *et al*. (2018) shown in Appendix VII.

3.3 Assessment of hypoxia reversal

3.3.1 Ethical Approval

The study design was approved by the Institutional Human Ethics Committee (IHEC) at Avinashilingam University (AUW/IHEC/BT-21-22/XMT-01). All the experiments were performed in accordance with relevant guidelines and regulations.

3.3.2 Sample collection

Fresh blood samples (5.0 ml) were obtained from healthy volunteers, using ethylene diaminetetra acetic acid (EDTA) as anticoagulant on the day of the experiments.

3.3.3 Isolation of lymphocytes

Lymphocytes are good model cells to study cellular responses. Separation of mononuclear cells is commonly performed in batch processes either by density gradient centrifugation or red blood cell (RBC) lysis and centrifugation (Urbansky *et al*., 2017). The major advantage of the red blood cell lysis method is that it is simple and requires a small volume (as little as 0.5 mL) of blood with a high success rate and high cell viability. The red blood cell lysis method avoids the mechanical centrifugal force in the process of density gradient centrifugation, which causes non-repairable damage to the cells. It is suggested that the red blood cell lysis method is more suitable for genetic and functional studies, which requires large numbers of cells as quickly as possible (Liu *et al*., 2017). Therefore, in the present study, peripheral blood lymphocytes were isolated from human blood using the RBC lysis method following the procedure by Dagur, (2015) as shown in Appendix VIII.

3.3.4 Induction of Hypoxia using Cobalt Chloride:

Several methods are used to induce hypoxia in cells such as modular incubator chamber, $CoCl_2$ method (Wu and Yotnda, 2011), Glucose Oxidase (GOX)/Catalase (CAT), medium height method (Rinderknecht *et al*. 2021), etc.

Among these, Cobalt chloride, a commonly used hypoxia-mimetic agent, artificially induces hypoxia and can block the degradation and thus induce the accumulation of HIF-1αprotein. Many reports have indicated that both cobalt chloride and hypoxia regulate a similar group of genes on a global gene expression level (Bae *et al*., 2012). Therefore, in the present study, acute hypoxic conditions were induced in isolated lymphocytes using cobalt chloride. A stock solution of 2.5mM cobalt chloride was prepared. Hypoxia was induced in lymphocytes by using cobalt chloride method followed by Wu and Yotnda (2011) as shown in Appendix IX.

3.3.5 Cell viability: Trypan Blue assay

The dye exclusion test is used to determine the number of viable cells present in a cell suspension. It is based on the principle that live cells possess intact cell membranes that exclude certain dyes, such as trypan blue, Eosin, or propidium, whereas dead cells do not. The trypan blue assay is quantitative, giving an "absolute" quantification because, through the cell-to-cell count, it has the estimated number of viable cells (Strober, 2001). Therefore, in the present study, viability of the isolated peripheral blood lymphocytes was assessed by using trypan blue assay following the protocol by Freitas *et al.* (2014) as shown in Appendix X.

3.3.6 Assessment of hypoxia reversal by SCMC-ONB treatment

To assess whether the oxygen nanobubbles have the potential to reverse acute hypoxia induced in isolated peripheral blood lymphocytes, oxygen nanobubbles are mixed with acute hypoxic lymphocytes at Room Temperature at pH 7.4 and incubated for 3 hours.

Cell viability was considered as the parameter for assessing hypoxia reversal. Cell viability was analyzed by Trypan blue assay as described in section 3.3.5.

Table 2

Experimental Setup

S.No	Sample	Volume of cells (µl)	Volume of PBS pH 7.4 (µl)	Volume of cobalt chloride (µl)	Volume of SCMC-ONB (µl)
1.	Control	10	190	-	-
2.	$CoCl_2$ control	10	189.75	0.25	-
3.	ONB treatment 1	10	189.75	0.25	50
4.	ONB treatment 2	10	189.75	0.25	100

3.3.7 Statistical Analysis

GraphPad Prism software was used for statistical analysis and graphical representations of the data. T-Tests were performed on the data and significance was checked. Nonsignificant values have been shown as ns in the results section, while *, **, *** and **** describe p values of less than <.5, .01, .001 and .0001, respectively.

Results and Discussion

4.0 RESULTS AND DISCUSSION

Oxygen (dioxygen, O_2) is mandatory to support human life from an early fetal stage onwards and for normal cellular function, as it is part of the electron transport chain for energy production in cells (Berner, 2007).

Oxygen plays an essential role in the respiratory process that drives the metabolisms of most living things (Chen *et al.*, 2020). To maintain homeostasis, the amount of oxygen within the tissues should respond to a gradient of pressure that pushes oxygen by diffusion throughout the membranes into the tissues (Prado *et al*., 2010). Excess oxygen can be toxic to cells due to increased levels of damaging reactive oxygen species (Zenewicz, 2017).

Hypoxia is a state of low oxygen content and partial pressure in the cell. All nucleated cells can sense oxygen concentration and respond to reduced oxygen availability. When oxygen delivery is disrupted or reduced, the organisms will develop numerous adaptive mechanisms to facilitate cell survival in the hypoxic condition. Normally, such hypoxic response will cease when oxygen level is restored (Chen *et al.*, 2020). Hypoxia, as one of the severe cellular stresses, can cause cellular injury and even cell death. Therefore, it is imperative to rescue or reverse acute hypoxia to prevent cell death in the event of acute hypoxemia and hypoxia (Al Tameemi *et al*., 2019).

Potential of oxygen nanobubbles to reverse acute hypoxia in isolated peripheral blood lymphocytes have been investigated in the present study.

The Results and Discussion pertaining to the study entitled **"Assessing the ability of sodium carboxymethyl cellulose oxygen nanobubbles to reverse acute hypoxia in isolated peripheral blood lymphocytes"** is discussed under the following headings.

4.1 Synthesis of sodium carboxy methyl cellulose oxygen nanobubbles (SCMC-ONB) by sonication method

4.2 Characterization of SCMC- ONB

4.2.1 Field Emission Scanning Electron Microscope (FESEM)

4.2.2. Energy Dispersive X-ray spectroscopy (EDX)

4.2.3 Fourier transform Infrared Spectroscopy (FTIR)

4.2.4 Three Dimensional Optical Profiler (3D Optical profiler)

4.2.5 XRD - X-ray diffraction

4.2.6 Dissolved Oxygen Content

4.3. Assessment of Hypoxia reversal

4.3.1 Assessment of hypoxia reversal by SCMC- ONB 3

4.1 Synthesis of sodium carboxy methyl cellulose oxygen nanobubbles (SCMC-ONB) by sonication method

In the present study, synthesis of oxygen nanobubbles was carried out by using sodium carboxymethyl cellulose polymeric shell by sonication method. The synthesis was carried out three different times with different settings as presented in Table 2. The Sodium Carboxy Methyl Cellulose Oxygen Nanobubbles obtained by using ultrasonication at different time periods are shown in Figure 3.

Figure 3

Sodium carboxymethyl cellulose oxygen nanobubbles

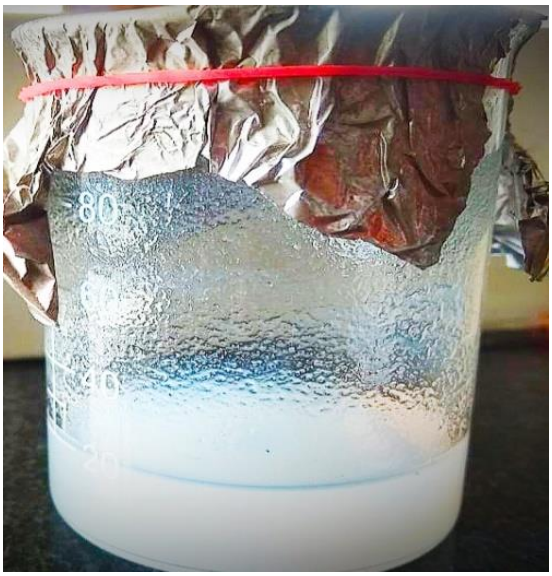

Researchers have used sonication in the range of 100 to 200 W for approximately 1 to 5 min in a pulsed mode to create MNBs (McEwan *et al*., 2015 and Khan *et al.*, 2018). Commercial sonicators like bath-tub and tip sonicators are also available for synthesizing MNBs. The limitation of the sonication method is the productivity and yield of the MNBs. This is because only a limited amount of solutions can be sonicated within a given time. Therefore, researchers have investigated other methods for a high yield (Kheir *et al.*, 2013).

4.2 Characterization of SCMC-ONB

4.2.1 Field Emission Scanning Electron Microscope (FESEM)

Scanning electron micrographs of the SCMC-ONB produced. FESEM images show surface morphology and size of the SCMC-ONB. Figure 4 a) shows 2400X magnification. From the image it can be observed that the size is less than 20 micron. In the lower left panel, individual SCMC-ONBs are observed in cylindrical shape, but in the upper right part of the image clumping of SCMC-ONBs is observed. Figure 5b, 5c and 5d show the same SCMC-ONBs in 5000X, 10000X and 20000X magnifications.

Khan *et al.* (2018) reported that the core–shell nature of the bubbles is evident in the bubbles having a diameter of ∼5 μm or more, indicating that ONBs are most likely to have a similar core–shell nature. SEM image of a microbubble with a size of 4.3 μm with spherical shape is clearly observed. Kim *et al.* (2021) examined the enamel structure of calcified teeth under hypoxic conditions and ONBs treatment using scanning electron microscopy. The enamel of teeth in normoxia showed a solid structure as enamel rods, whereas the enamel rods of teeth under hypoxic conditions were disorganized, and many pores were observed. Crystallization was very low under hypoxic conditions compared to that under normoxic conditions.

From the images from the FESEM, it is observed that SCMC-ONB 3 are not spherical in shape but of cylindrical shape. Inclusion of surfactants might have been beneficial to minimize the clumping of SCMC-ONBs.

Figure 4

a) FESEM image of SCMC- ONB 3

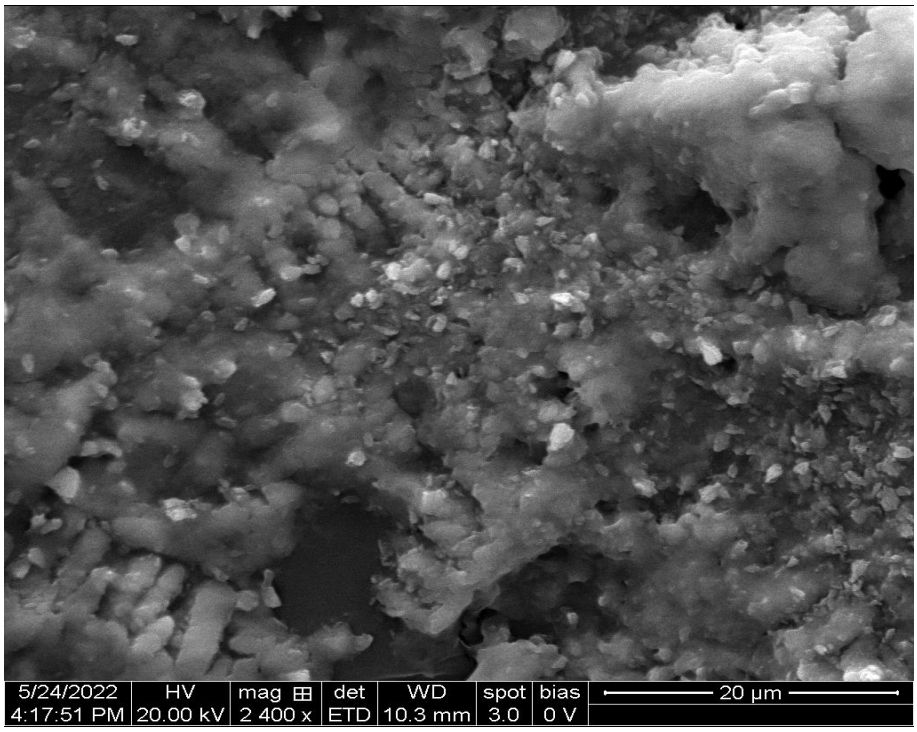

Figure 4

b) FESEM image of SCMC- ONB 3

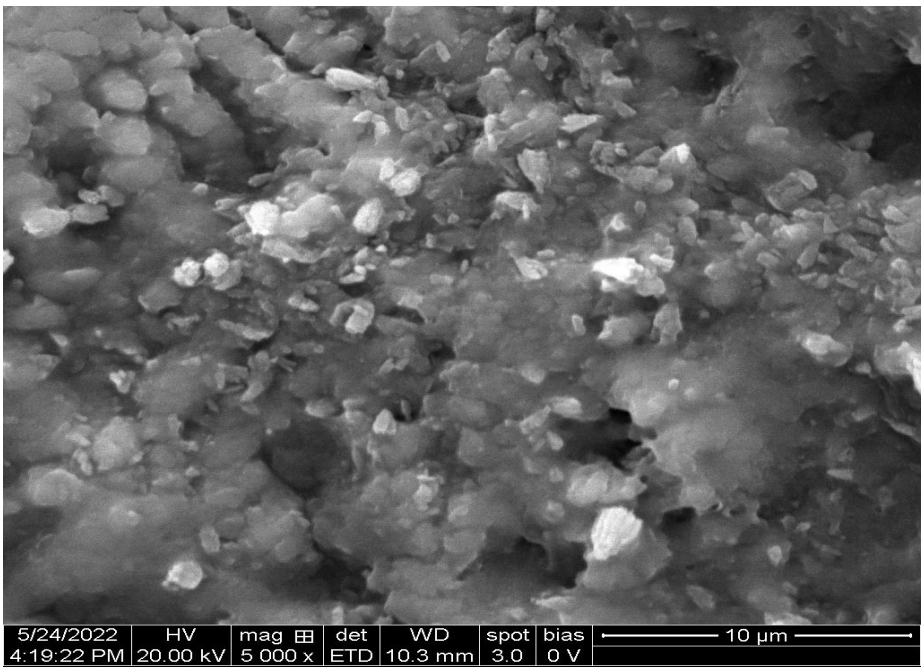

Figure 4

c) FESEM image of SCMC- ONB 3

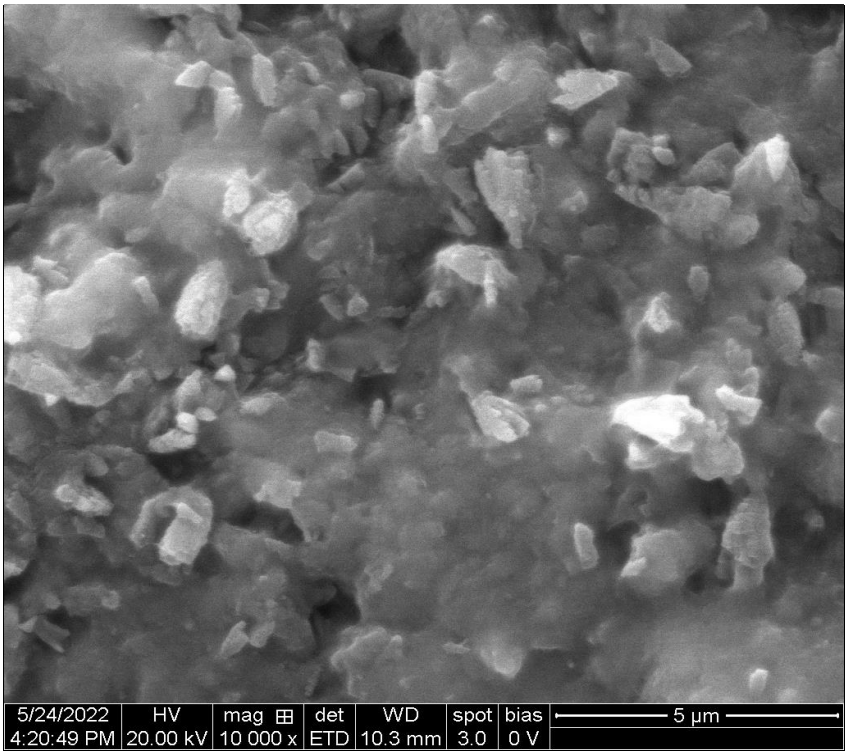

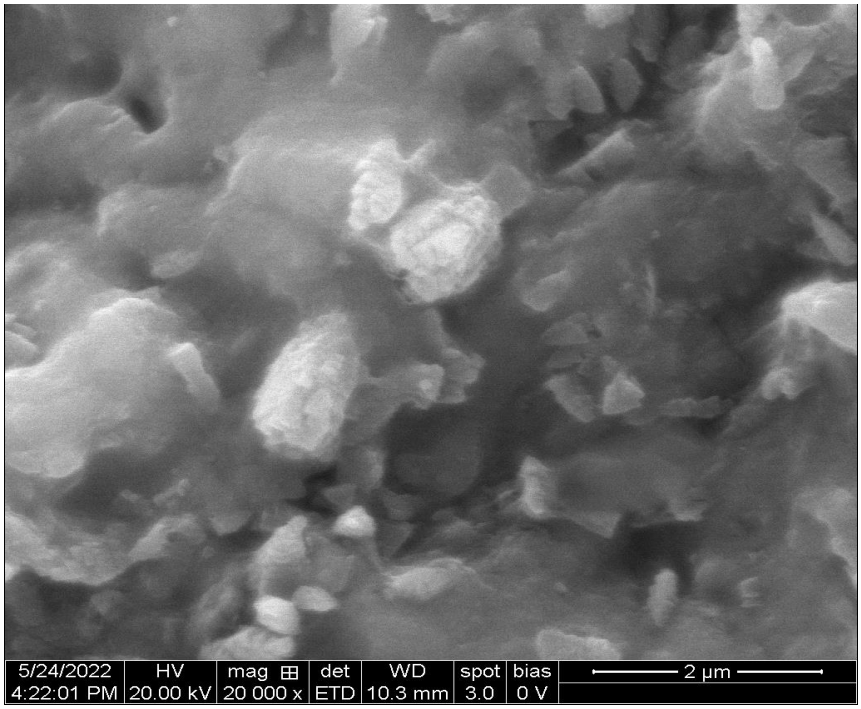

Figure 4

d) FESEM image of SCMC- ONB 3

4.2.2. Energy Dispersive X-ray spectroscopy (EDX)

Elemental composition of SCMC- ONB 3 was assessed by EDX and is presented in Figure 5 and Table 3.

Figure 5

Graphical representation of EDX image for SCMC- ONB 3

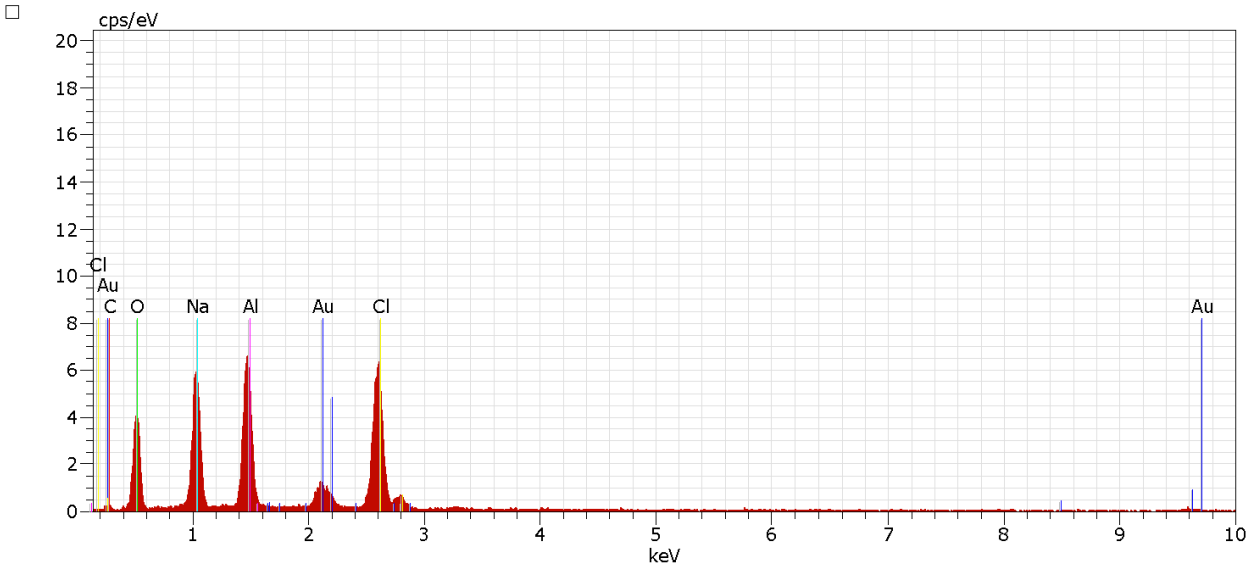

Table 3

Elemental composition of SCMC- ONB3

Series = characteristic X-ray lines; unn. C [wt.%] = the unnormalised concentration in weight percent of the element ; norm. C [wt.%] = the normalized concentration in weight percent of the element; C Atom. [at.%] the atomic weight percent; C Error (1 Sigma) [wt.%) = the error in the weight percent concentration at the 1 sigma level

S.No	Element	Atomic Number	Series	Unn. C [wt.%]	Norm. C [wt.%]	C Atom [at.%]	C Error (1 Sigma) [wt.%]
1.	O	8	K-series	34.71	35.11	47.61	5.66
2.	Na	11	K-series	18.64	18.86	17.80	1.29
3.	Cl	17	K-series	17.09	17.29	10.58	0.64
4.	Al	13	K-series	15.41	15.59	12.54	0.81
5.	Au	79	K-series	7.17	7.25	0.80	0.36
6.	C	6	K-series	5.84	5.91	10.67	2.22
			Total:	98.87	100.00	100.00	

From Figure 5 and Table 3, it is evident that as expected, the percent weight of Oxygen of SCMC- ONB 3 is highest among all elements. Sodium and carbon are present in SCMC-ONB as part of the polymer, aluminum and chlorine act as a crosslinking agent and used to prevent size reduction of SCMC-ONB 3. Gold is not present in SCMC-ONB 3, but was used as a sputter coater for EDX analysis. So it shows up in the analysis.

Kim *et al*. (2021) have reported that quantitative analysis of the enamel and dentin using energy dispersive spectroscopy (EDS) revealed that both the enamel and dentin were mainly composed of Ca, P, O, and C under normoxic conditions. Ca and P levels were decreased in the enamel of teeth under hypoxic conditions, whereas in the dentin of teeth levels of Ca, P, O, and C were increased under hypoxic conditions. Keller *et al.,* (2019) have revealed that from an EDX point analysis in each of the centers of the two shells obtained are 11.2 wt% O and 88.8 wt% Pt for the inner as compared to 2 wt% O and 98 wt% Pt for the outer shell of the bubble, assuming that only these two elements are present. In atomic ratios this converts to x = 1.25 in PtOx for the inner shell, compatible with a Pt3O4 stoichiometry.

From EDX analysis, the composition of SCMC- ONB 3 are oxygen (O), sodium (Na), chlorine (Cl), aluminum (Al), and carbon (C) was confirmed.

4.2.3 Fourier transform Infrared Spectroscopy (FTIR)

The Fourier transform Infrared Spectroscopy (FTIR) results estimating the functional group of the SCMC-ONBs 1, 2 and 3 are depicted in Figure 6.

Figure 6

FTIR Spectrum of SCMC-ONB 3

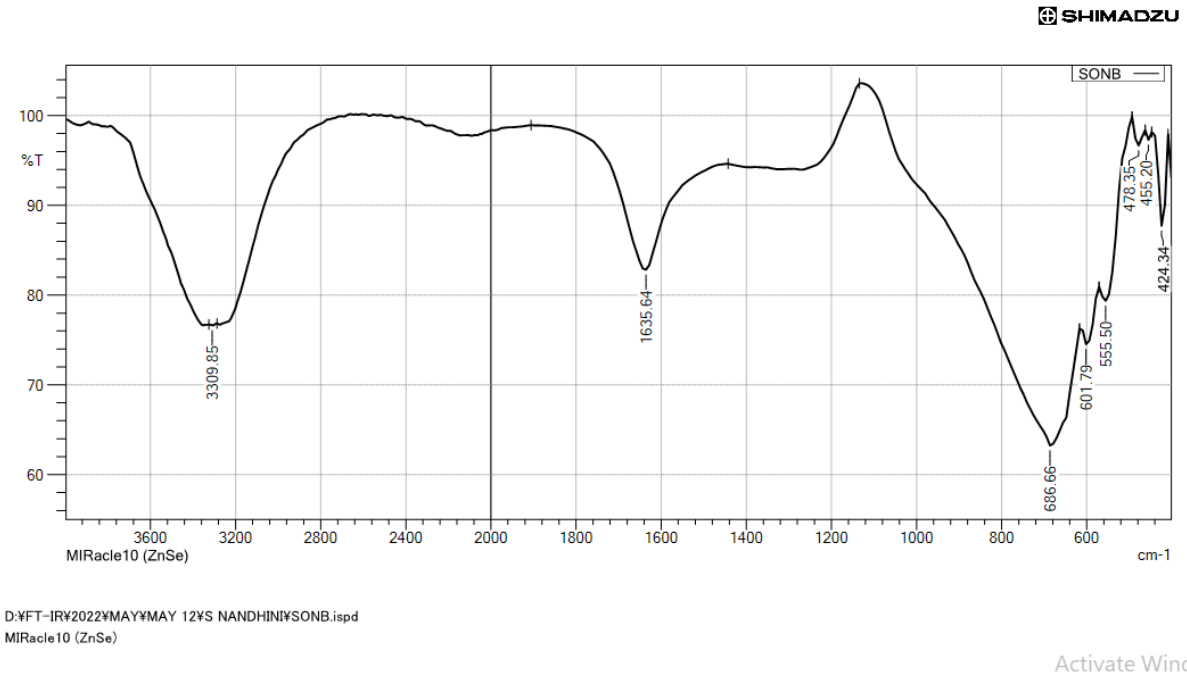

FTIR spectrum of SCMC- ONB3 shows three major peaks. The peak at 3309.85 cm-1 corresponds to hydroxyl group, H-bonded OH stretch. Alkenyl C=C stretch are related with wavenumbers 1635.64 cm^{-1} or it might correspond to amide or primary amine, NH bend or secondary amine, >N-H bend or Open-chain imino (-C=N-) or Organic nitrates. Wavenumber 686.66 cm^{-1} and 601.79 cm^{-1} indicates aliphatic bromo compounds, C-Br stretch or Disulfides (S-S stretch) or alcohol, OH out-of-plane bend. The 555.50 cm^{-1} band corresponds to aliphatic iodo compounds, C-I stretch. The wavenumber 478.35 cm^{-1} and 455.20 cm^{-1} indicates Aryl

disulfides (S-S stretch) and 424.34 cm^{-1} wavenumber related to fingerprint region. From the spectrum, we may conclude that SCMC-ONB3 may contain hydroxyl group (OH), an alkene (C=C) or amine (NH) or imines (-C=N-), aliphatic bromo compounds (C-Br) or disulfides (S-S) and aliphatic iodo compounds (C-I) at different frequencies. All these functional groups are part of the carboxy methyl cellulose which is the major component of the SCMC-ONB3.

Oh and Kim, (2017) states that the ATR-FTIR spectrum of the BNBs in water clearly shows that the shape and position of the band matched the gaseous CO2 spectrum. The recorded IR spectrum shows two branches with fine lines at about 2300−2380 cm^{-1} and shape changes in the spectrum are attributed to the high resolution. In addition, in a different experiment, we also obtained the IR spectrum of dissolved CO2 molecules in DI water. Before measuring the IR spectrum, CO2-saturated water was prepared; a saturated condition for CO2 gas dissolution is created at 1.0−1.2 bar. Unlike the BNBs in water, the obtained IR spectrum from the CO2-saturated water showed a single peak at 2343 cm^{-1}. Similarly, Zhang *et al.,* (2007) performed ATR-FTIR spectroscopy to reveal the gas content of the surface nanobubbles; the recorded ATR-FTIR spectrum is the same as that of CO2 gas. As a result, the obtained ATR-FTIR spectrum of the BNBs reveals that the generated BNBs in water were filled with gaseous CO2 molecules

4.2.4 Three Dimensional Optical profiler

The 3D optical profile results showing surface height of the SCMC-ONBs 1, 2 and 3 are depicted in Figure 7a, 7b and 7c, respectively.

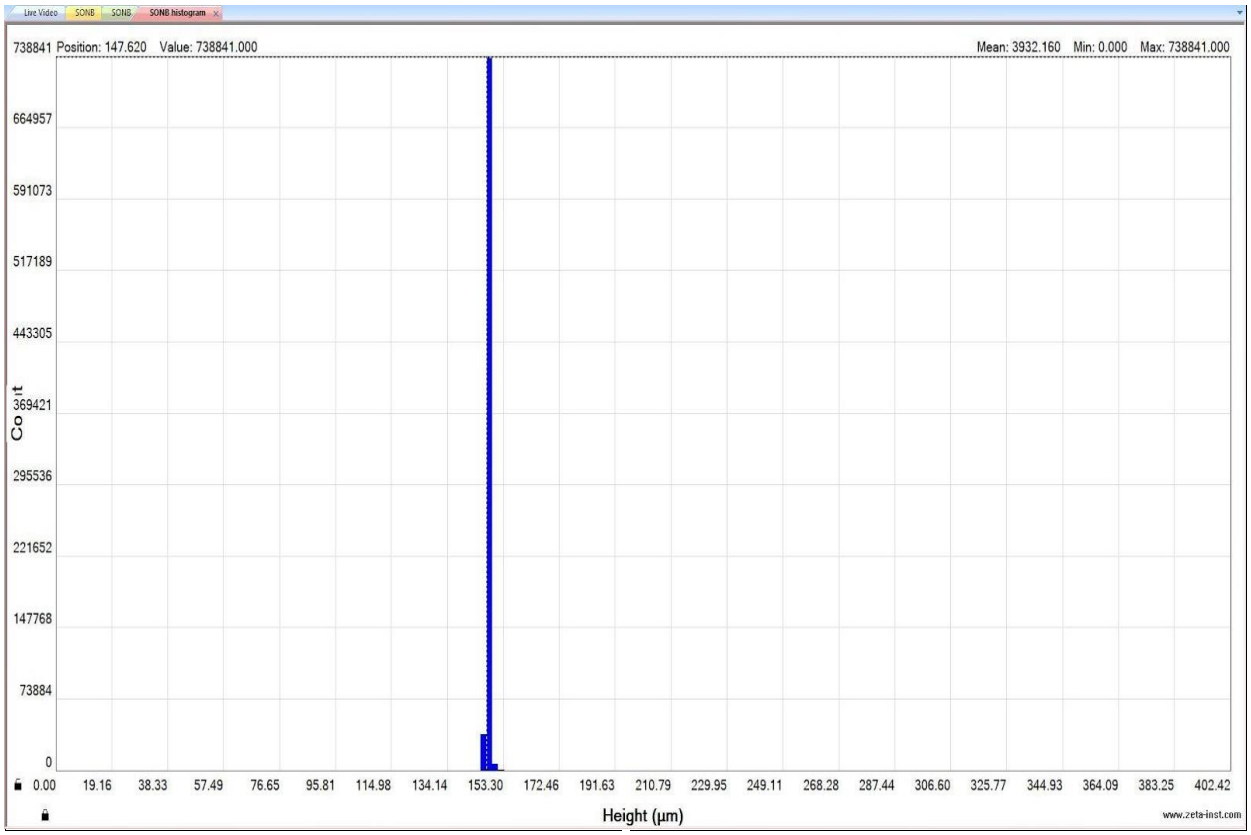

Figure 7

a) Surface height of SCMC-ONB 1

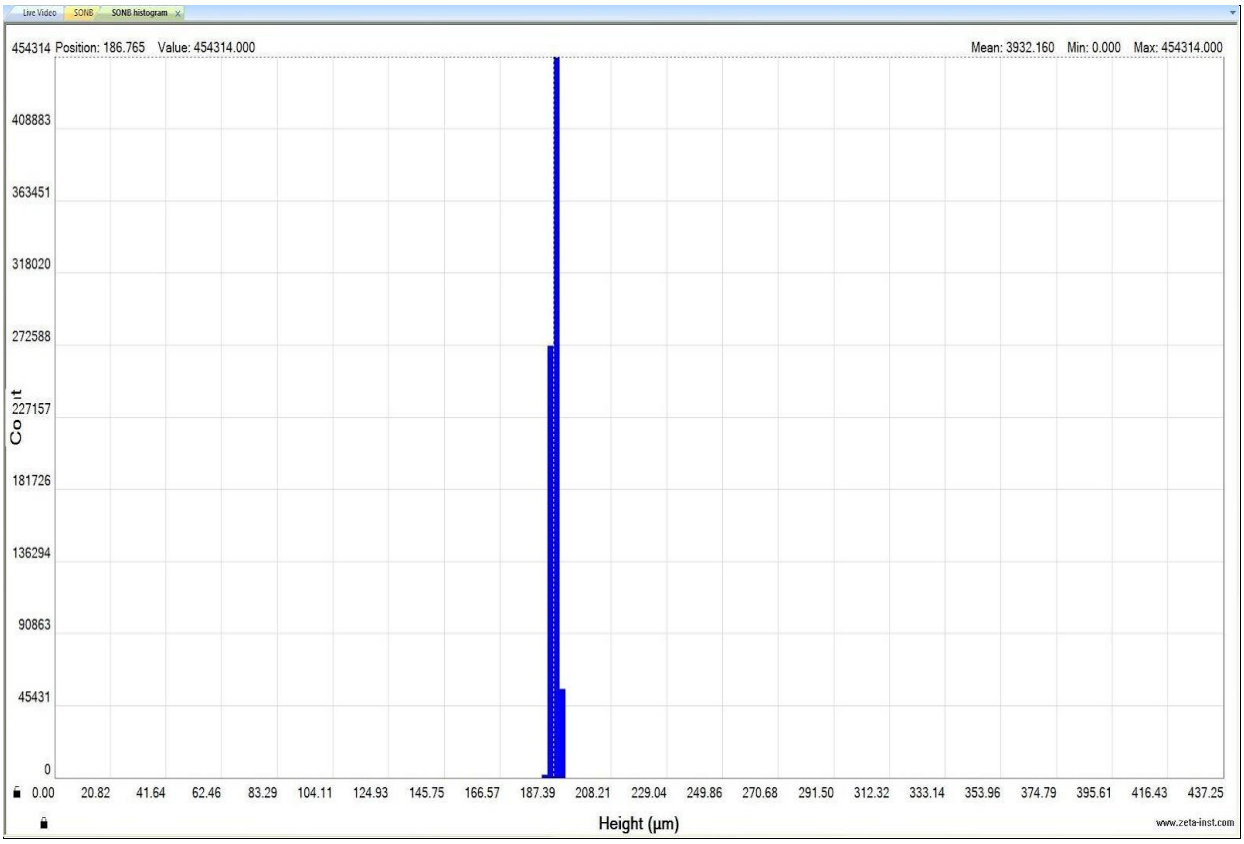

Figure 7

b)Surface height of SCMC-ONB 2

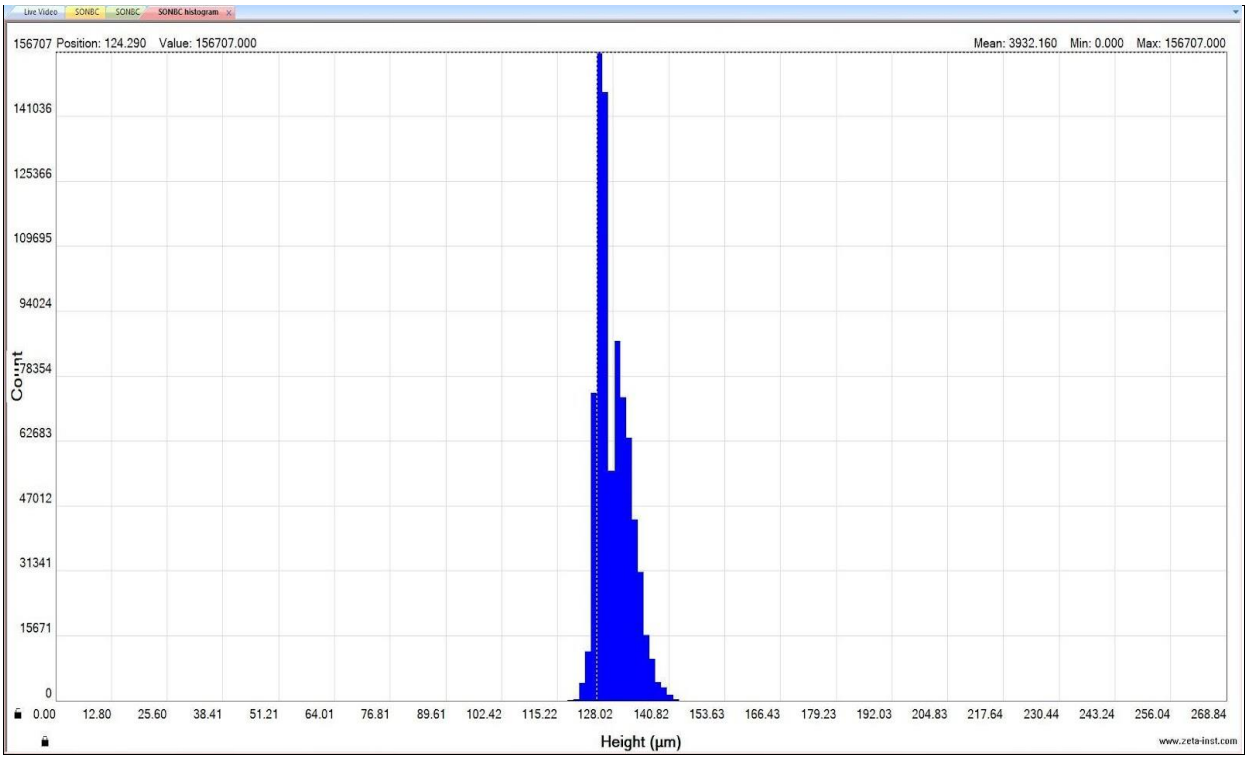

Figure 7

c)Surface height of SCMC-ONB 3

SCMC-ONB1 shows a single peak with a surface height 158 µm suggesting uniform surface height for all the nanobubbles. This also shows the nanobubbles are not clumped. SCMC-ONB 2 surface height was found to be uniform with a narrow range of approximately 185-190 µm. SCMC-ONB3 showed a decreased but wide surface height for the nanobubbles in the range of 125- 145 µm. The difference in the surface heights might be due to the influence of the sonication time on the nanobubbles. SCMC-ONB1 was sonicated for 60 minutes, SCMC-ONB2 for 120 minutes and SCMC-ONB3 for 5 minutes. As the time of sonication increased, the surface height of the nanobubble also increased. Lower the sonication period the surface height was also varied, whereas for longer periods of sonication the surface was narrow and uniform for the nanobubbles.

The 3D optical profile results showing surface area of the SCMC-ONBs 1, 2 and 3 are depicted in Figure 8a, 8b and 8c respectively.

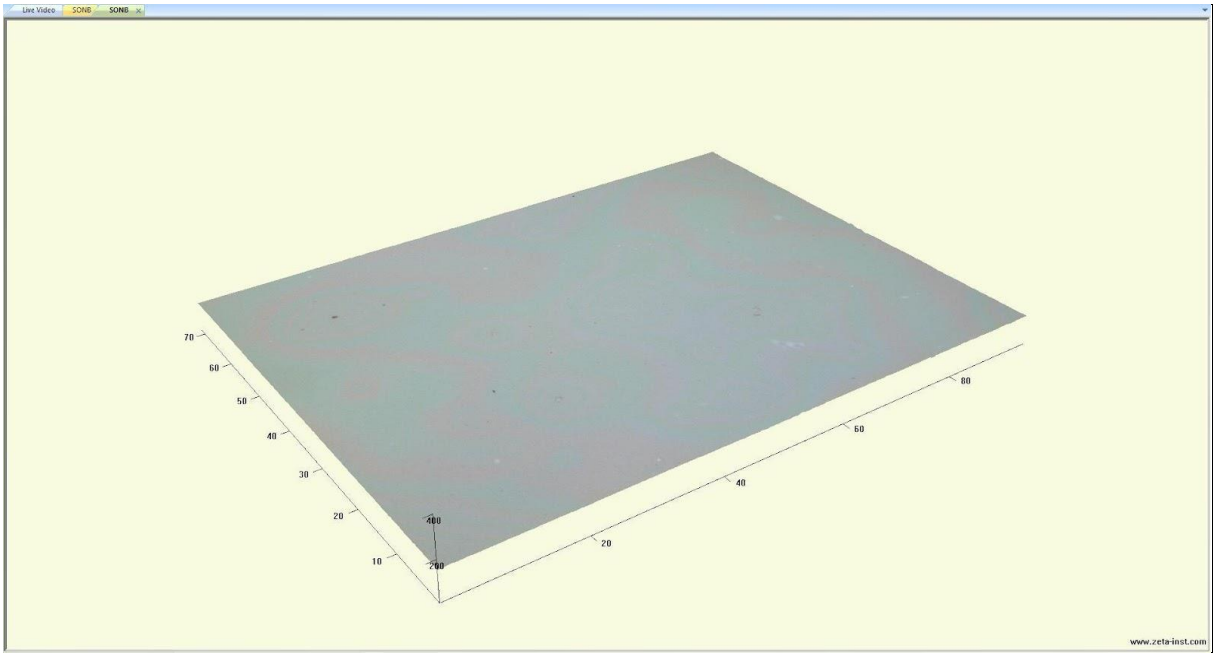

Figure 8

a)Surface area of SCMC-ONB 1

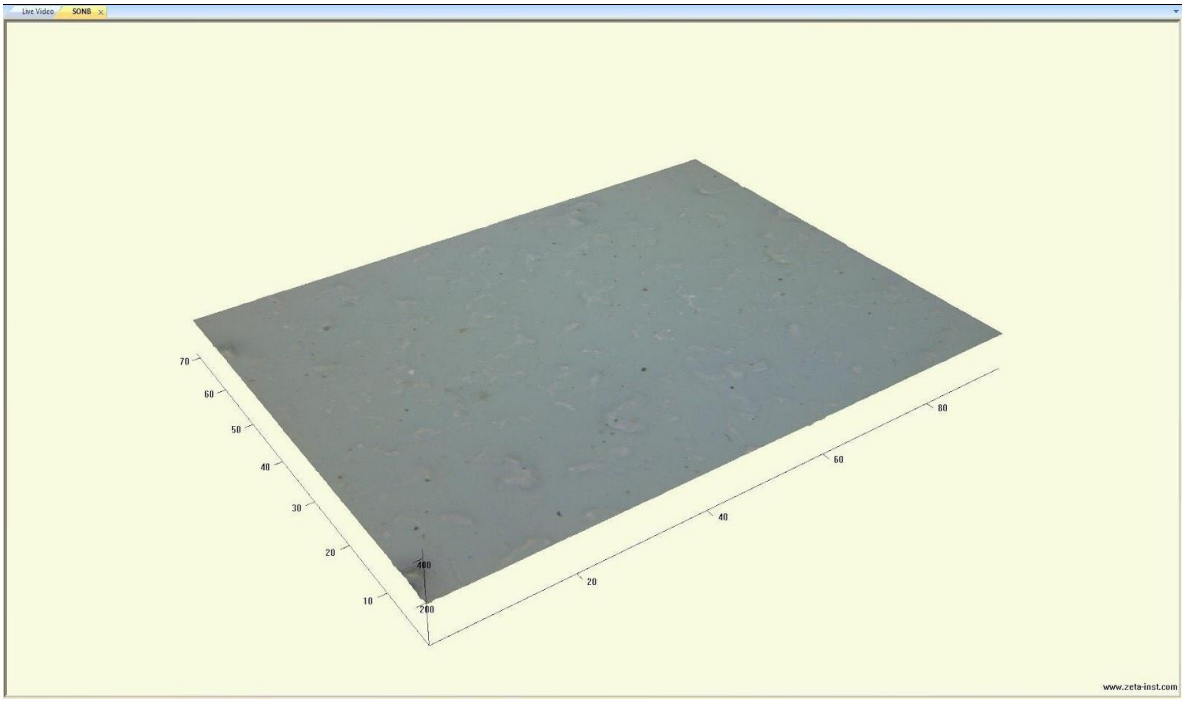

Figure 8

b)Surface area of SCMC- ONB 2

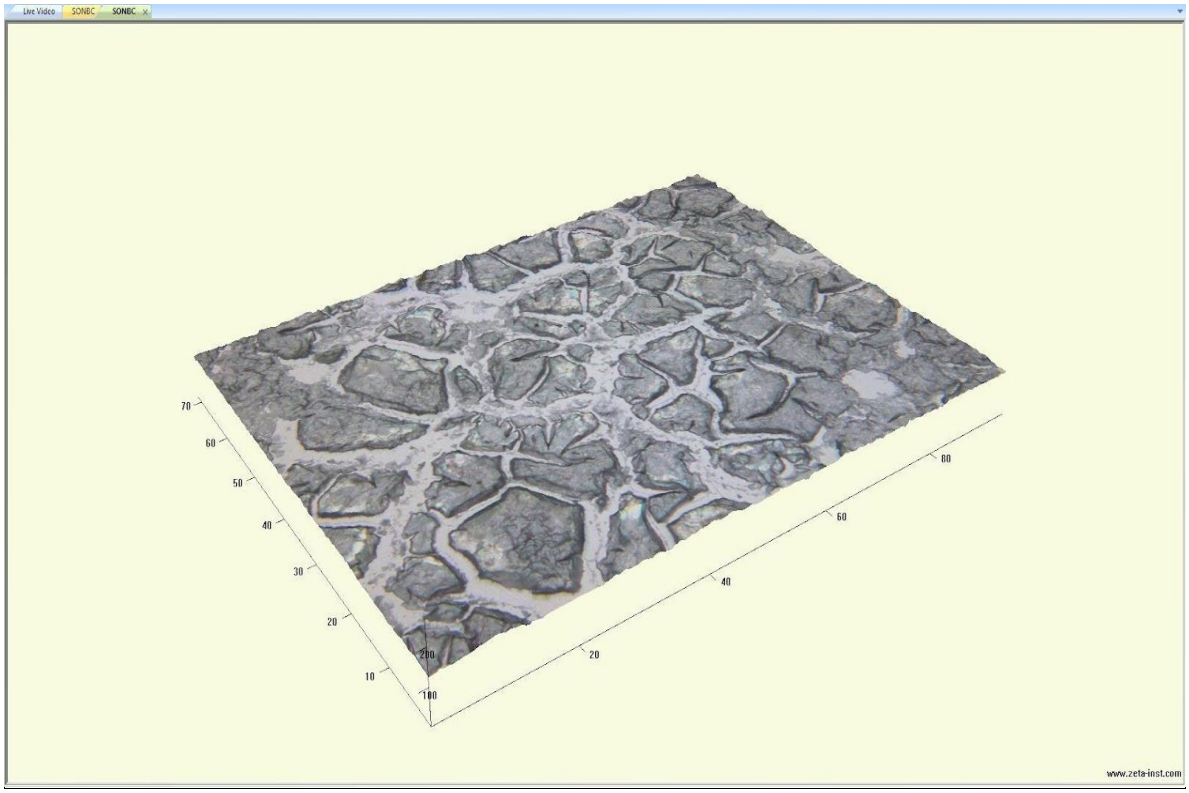

Figure 8

c)Surface area of SCMC- ONB 3

From the images of 8 a, b and c, it is evident that the surface area of SCMC-ONB1 is smooth and uniform when compared to the other two SCMC-ONBs. SCMC-ONB2 is rougher compared to SCMC-ONB1 whereas smoother compared to SCMC-ONB3. It is observed that as the time for sonication decreases, the surface area becomes rougher.

The 3D optical profile results showing surface area of the SCMC-ONBs 1, 2 and 3 are depicted in Figure 9a, 9b and 9c respectively in color. From the images in Figure 9, we can conclude that sonication time influences the surface smoothness and uniformity in the inverse way. As sonication time increases, surface smoothness of the nanobubbles decreases.

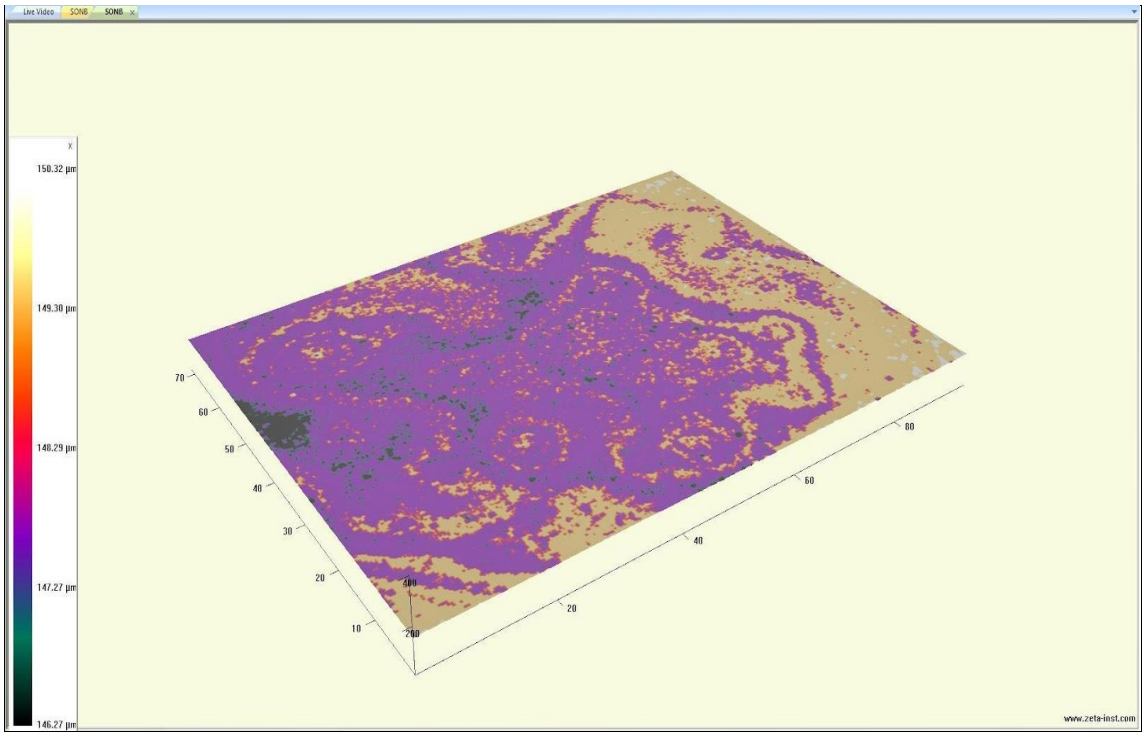

Figure 9 a) Surface displayed with multiple color options for SCMC- ONB 1

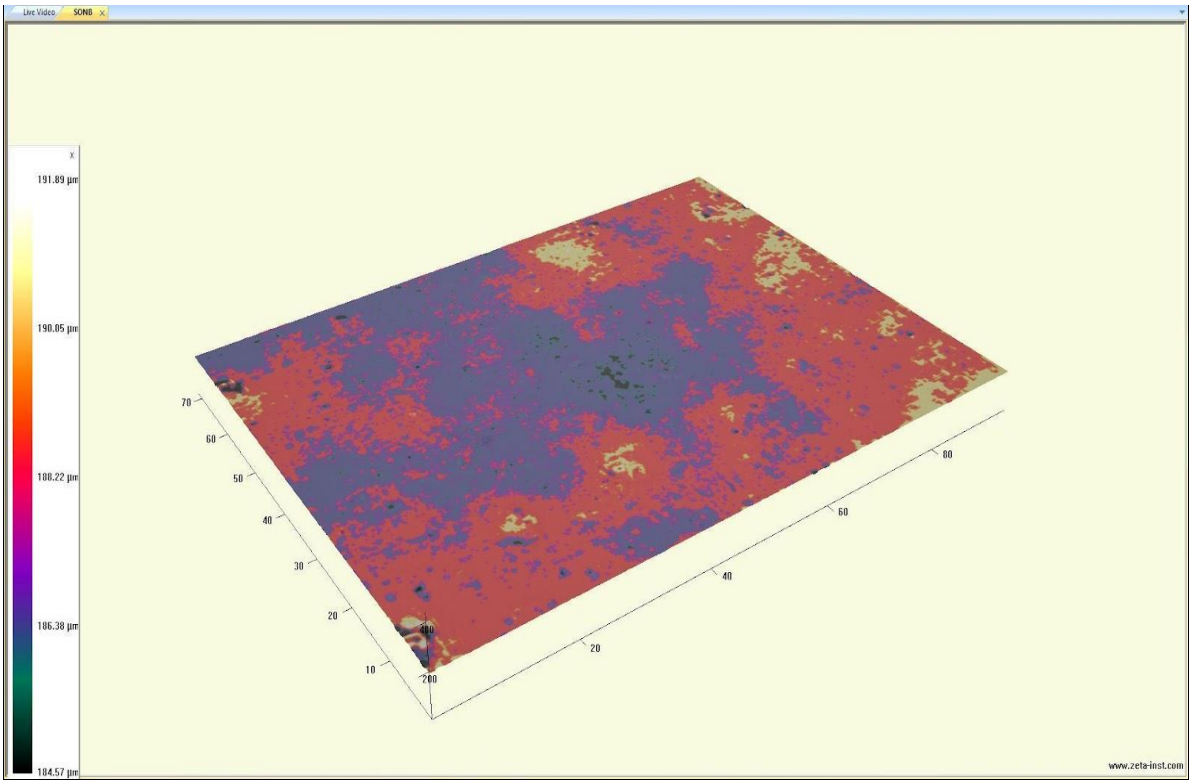

Figure 9 c)Surface displayed with multiple color options for SCMC- ONB 2

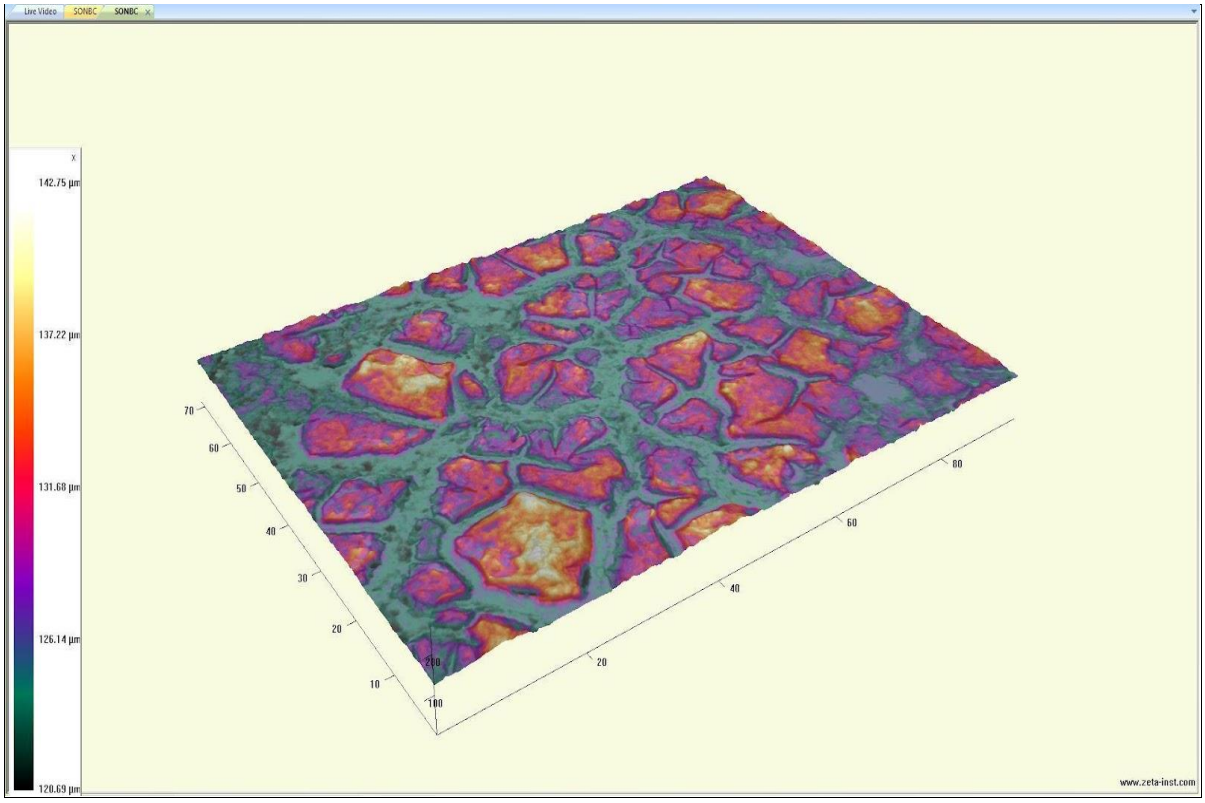

Figure 9 c)Surface displayed with multiple color options for SCMC- ONB 3

The 3D optical profile results showing average surface height SCMC-ONBs 1, 2 and 3 are depicted in Figure 10 a, 10b and 10c respectively.

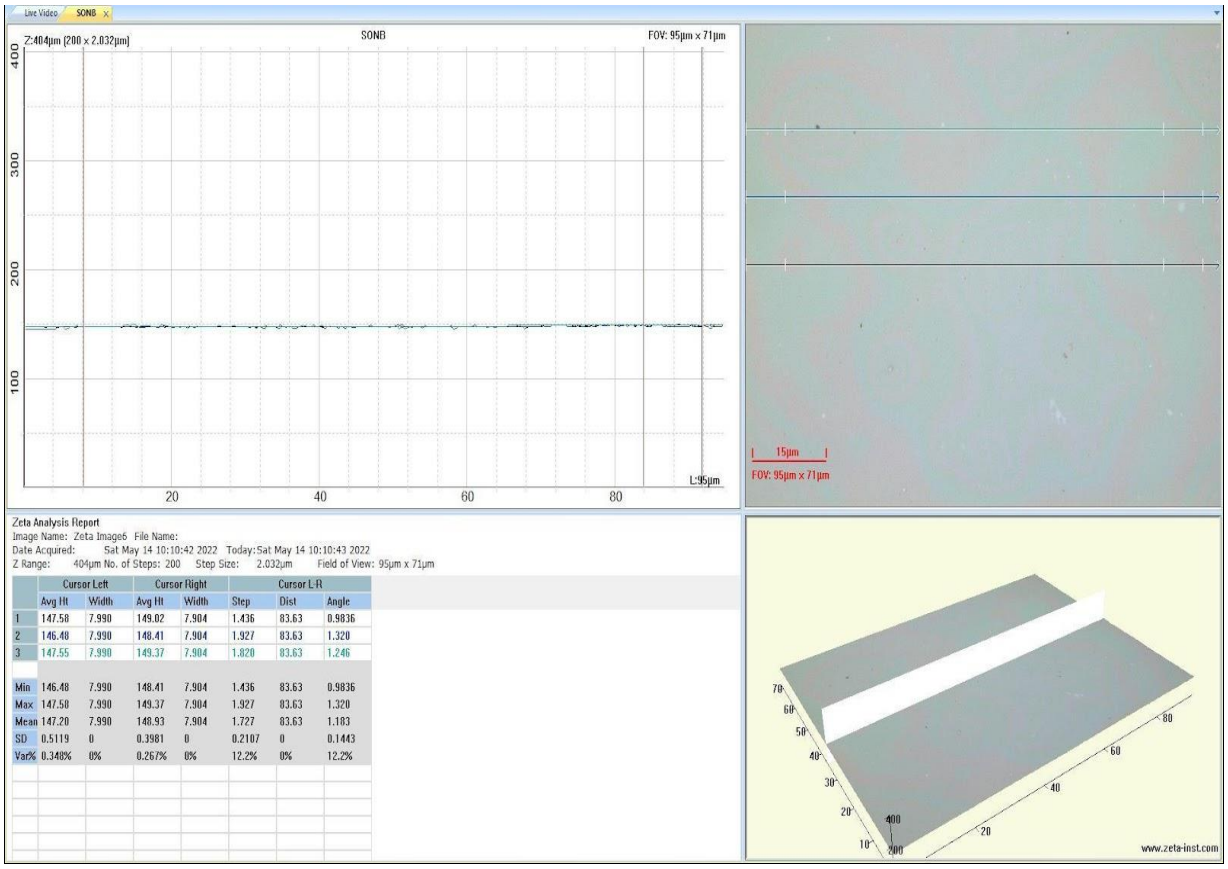

Figure 10

a) Multiple cross-section analysis for a sample SCMC-ONB 1

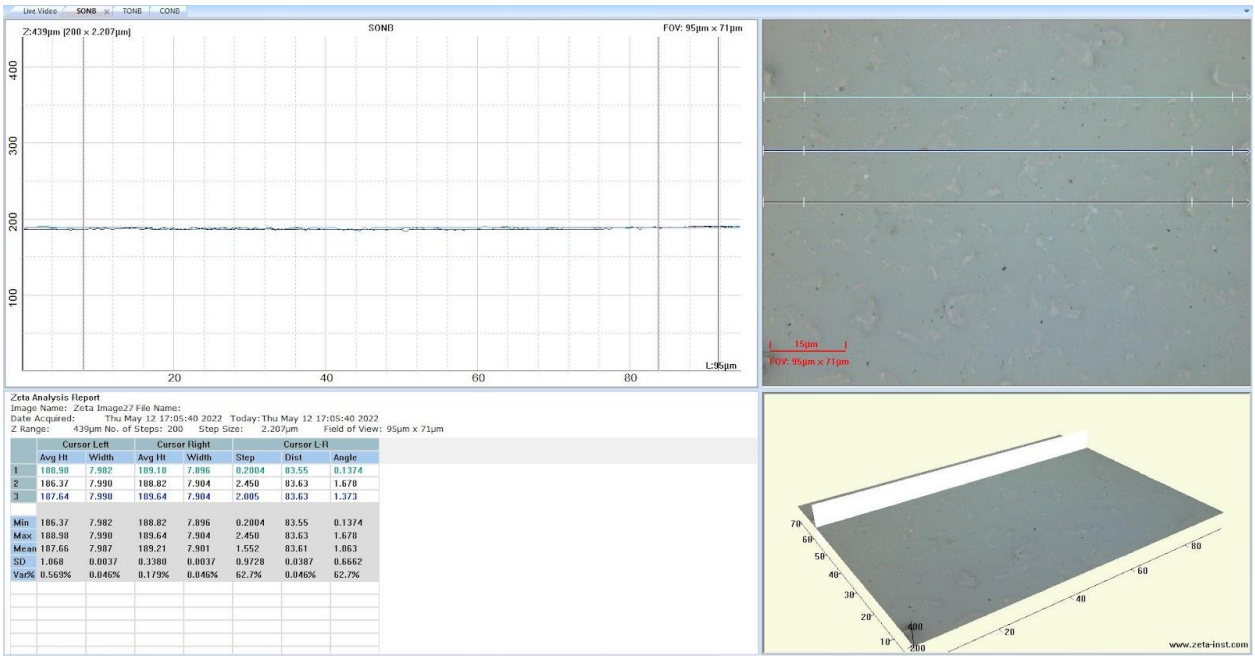

Figure 10 b)

Multiple cross-section analysis for a sample SCMC-ONB 2

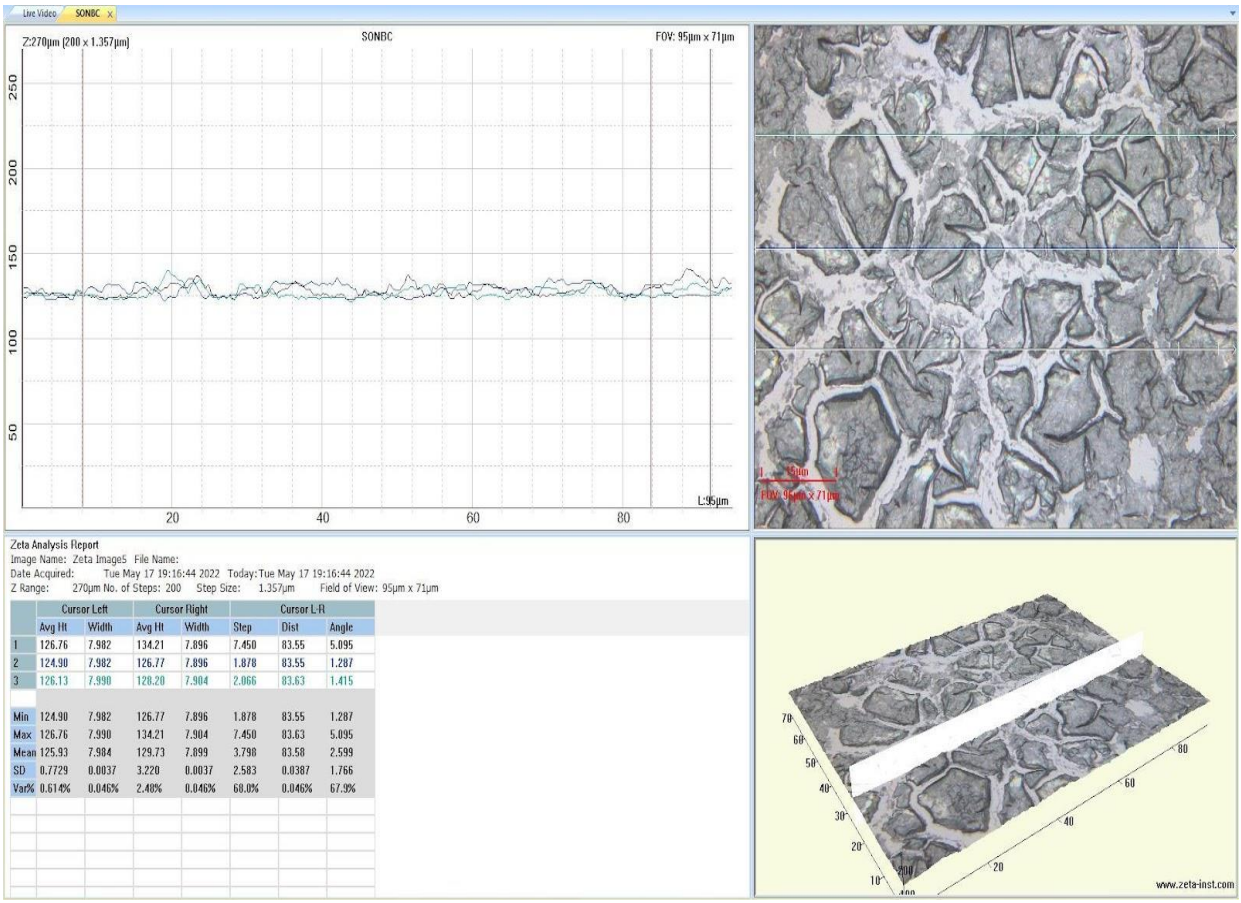

Figure 10

c)Multiple cross-section analysis for a sample SCMC- ONB 3

SCMC-ONB1 shows a single peak with an average surface height at 146-149µm suggesting uniform surface height for all the nanobubbles. This also shows the nanobubbles are not clumped. SCMC-ONB2 surface height was found to be uniform with a narrow range of approximately 185-190 µm. SCMC-ONB3 showed a decreased but wide surface height for the nanobubbles in the range of 125- 145 µm. The difference in the surface heights might be due to the influence of the sonication time on the nanobubbles. SCMC-ONB1 was sonicated for 60 minutes, SCMC-ONB2 for 120 minutes and SCMC-ONB3 for 5 minutes. As the time of sonication increased, the surface height of the nanobubble also increased. Lower the sonication period the surface height was also varied. There is no change in width and distance of SCMC-ONB 1 and 2. Slight changes of width and distance from SCMC-ONB 3.

Profile Leveling is performed in the profile window using the vertical cursors and cannot be done using markers as depicted in Figure 11 a), b) and c) for SCMC-ONBs 1,2 and 3 respectively.

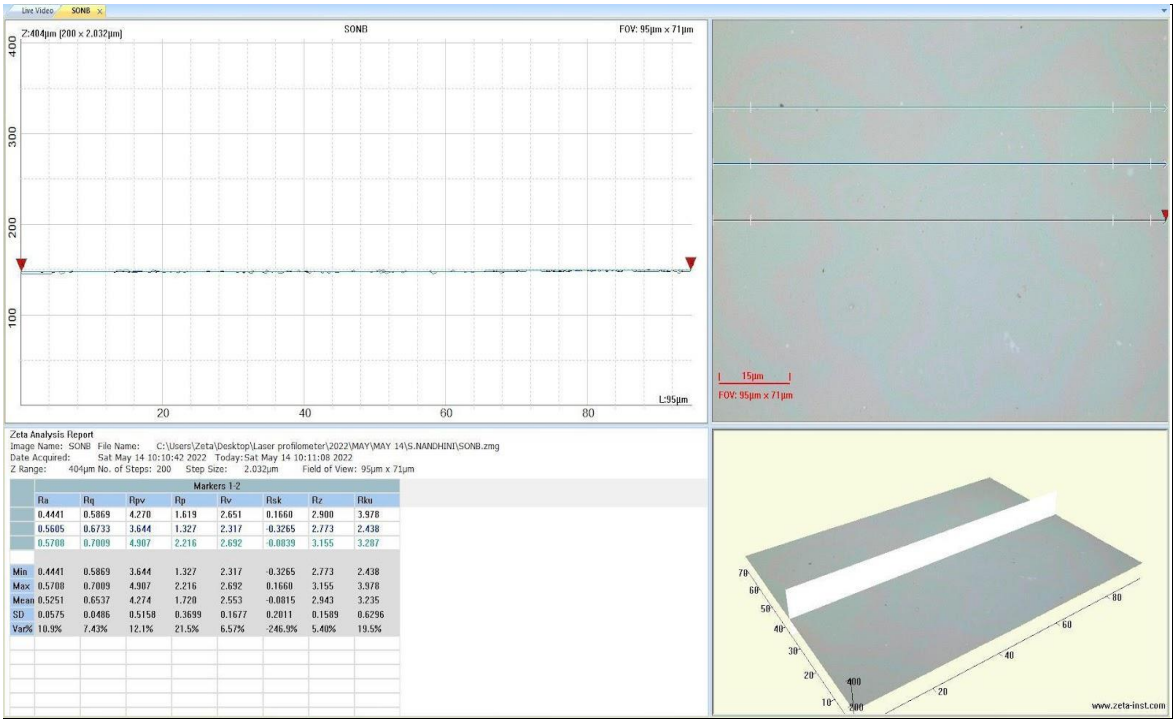

Figure 11 a) Illustrations of profile markers across multiple cross-sections for SCMC-ONB1

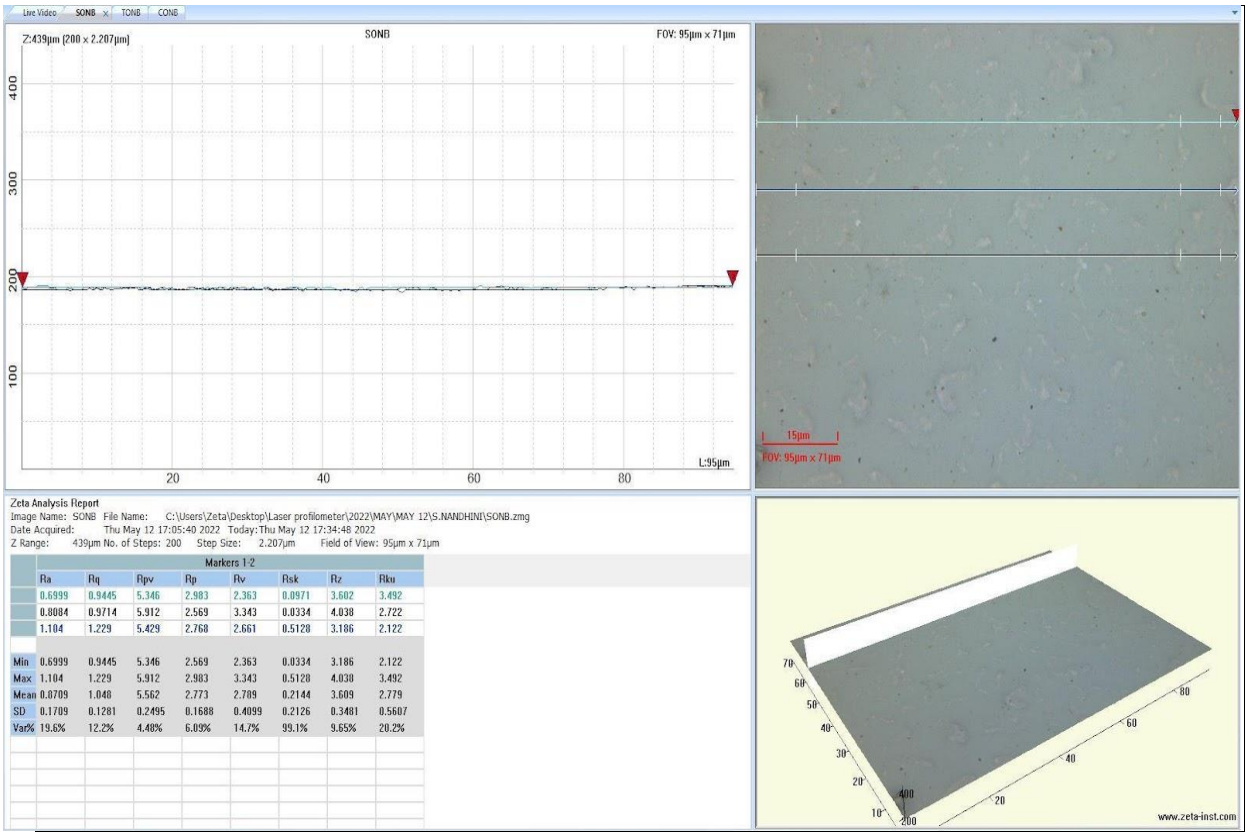

Figure 11

b) Illustrations of profile markers across multiple cross-sections for SCMC-ONB 2

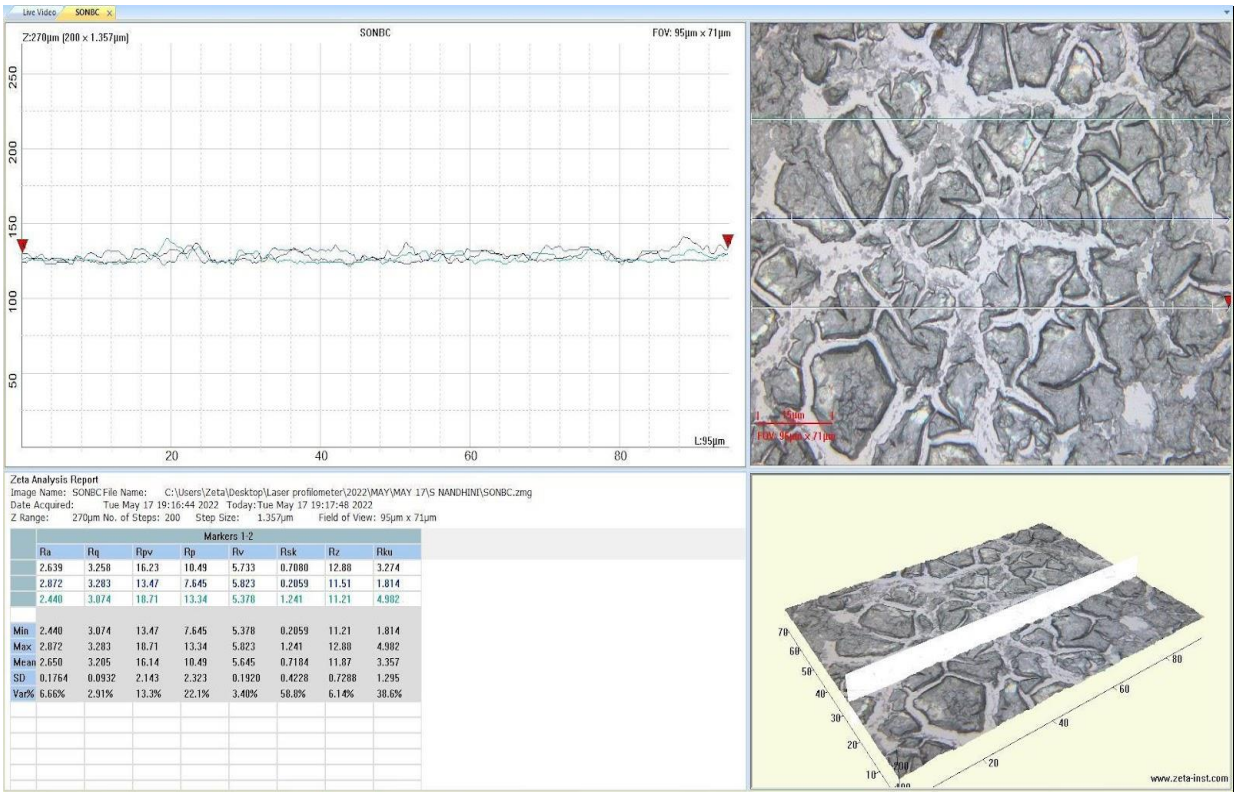

Figure 11

c)Illustrations of profile markers across multiple cross-sections for SCMC-ONB 3

Table : 4

Roughness parameters

S. No	Parameters	Definition
1.	Ra	Arithmetic average of deviations from the mean
2.	Rq	Room mean squared values of deviations
3.	Rpv	Maximum peak to valley difference
4.	Rp	Maximum peak height
5.	Rv	Aaximum valley depth
6.	Rz	Average of (Rp-Rv) from five sections

7.	**Rsk**	**Skewness (asymmetry of distribution)**
8.	**Rku**	**Kurtosis (shape of distribution peak)**

The Analysis Report displays the roughness parameter is usually used to characterize optical surfaces (more smooth)and Sa machined surfaces (more irregular). From the images of 11 a, b and c it is evident that SCMC-ONB3 is irregular when compared to the other two SCMC-ONBs. SCMC-ONB2 is regular compared to SCMC-ONB1 whereas regular compared to SCMC-ONB3. As the time of sonication increased, the roughness of the nanobubble also decreased and became smooth or regular. Lower the sonication period the nanobubbles are more irregular.

4.2.5 X-ray diffraction

X-ray diffraction (XRD) analysis results showing the crystallographic structure of SCMC-ONB and is presented in Figure 12.

Figure: 12

Graphical representation of XRD profiles of the SCMC-ONB 3

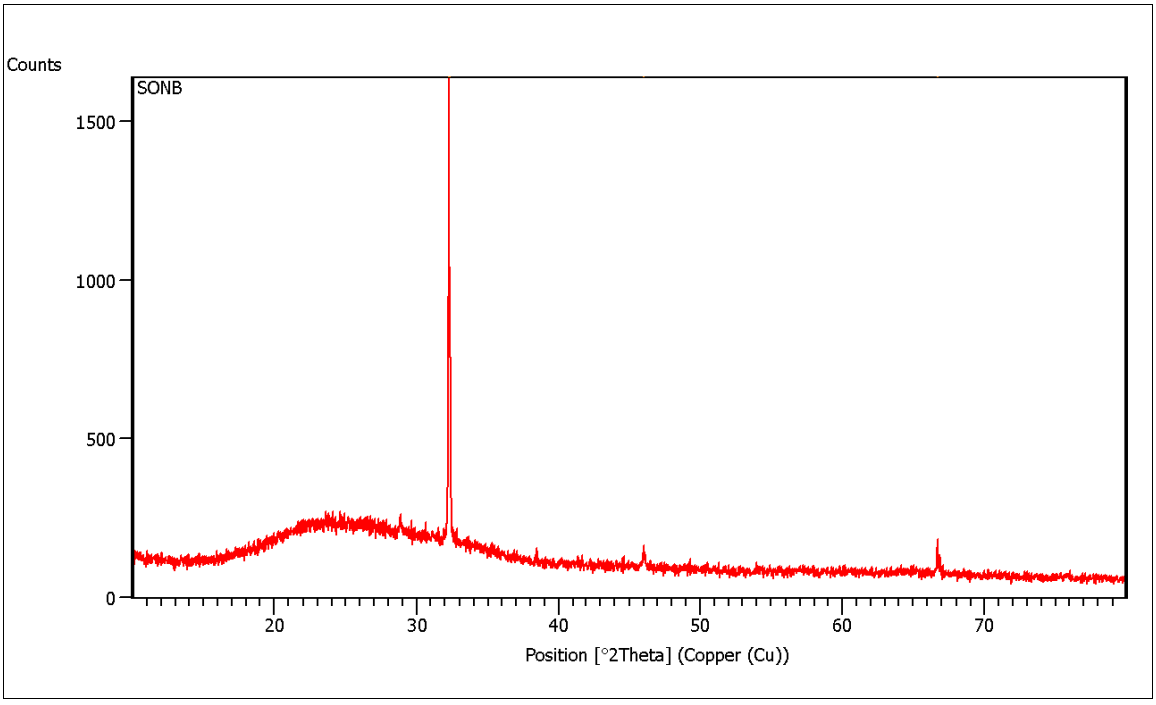

The X-axis shows the pattern is measured in 2θ and the y-axis is relative intensity of the diffracted beam. Sharp peaks in the XRD pattern indicate that SCMC-ONB3 is a crystalline material. The sharp and well defined Bragg peaks at specific 2θ value in the powder XRD pattern confirmed its crystallinity. The single peak indicates that SCMC-ONB3 is a single crystalline structure. XRD pattern of SCMC-ONB 3 displays four characteristic diffraction peaks located at 32.2°, 32.3° , 46.0° and 66.7°at 2θ. The strongest and sharpest diffraction peak at around 2θ was obtained are indexed as the reflection of crystalline structure in SCMC-ONB 3.

Pos. [°2Th.]=position of the peak, FWHM Left [°2Th.] full-width at half-maximum d-spacing [Å]-inter-atomic spacing and Rel. Int. [%]= Relative intensity

Table 5

Peak List

Pos. [°2Th.]	Height [cts]	FWHM Left [°2Th.]	d-spacing [Å]	Rel. Int. [%]
32.2934	1449.49	0.0612	2.76989	100.00
32.3880	799.32	0.0612	2.76888	55.14
46.0425	52.26	0.2448	1.96971	3.61
66.7243	112.30	0.0816	1.40072	7.75

Qi and Xin (2010) reveals that XRD patterns exhibited strong diffraction peaks at 27°, 36° and 55° indicating TiO2 in the rutile phase. On the other hand, in Figure 2, XRD patterns exhibited strong diffraction peaks at 25° and 48° indicating TiO2 in the anatase phase. All peaks are in good agreement with the standard spectrum (JCPDS no.: 88-1175 and 84-1286). From Figure 1 and Figure 2, they were shown that the diffraction pattern peak intensity of the TiO2 increases with increasing particle size. These results suggested that the nano-TiO2 powder is composed of irregular polycrystalline. Amorphous revealed a broad pattern with low intensity; however, the effect of the amorphous materials on the broadening of the XRD patterns of nanosized TiO2 is negligible.

4.2.6 Dissolved Oxygen Content

The oxygen concentration was measured by using a dissolved oxygen (DO) meter after injecting nanobubbles in deoxygenated water. In the present study, oxygen release property of SCMC-ONB3 was assessed at four different concentrations namely 10 µl, 25 µl, 50 µl and 100 µl. The results of the same are depicted in Table 6 a), b), c) and d) and Figure 14 a), b) c) and d) respectively. Paired Student's T test was performed to compare the release of oxygen over a period of 8 minutes in all the concentrations. It was found that no significant difference was found between the control and addition of SCMC-ONBs at all four concentrations. It may be concluded that SCMC-ONBs do not serve as good sources of oxygen as already observed.

Table 6

a) Dissolved oxygen concentrations for 10µl of SCMC-ONB 3

Time (minutes)	Dissolved Oxygen (mg/l)	
	Control	**10µl of SCMC-ONB 3**
0	**24.0**	**25.0**
1	**23.5**	**20.1**
2	**22.2**	**19.8**
3	**21.6**	**19.7**
4	**21.2**	**19.5**
5	**20.9**	**19.4**
6	**20.8**	**19.3**
7	**20.4**	**19.2**
8	**20.2**	**19.1**

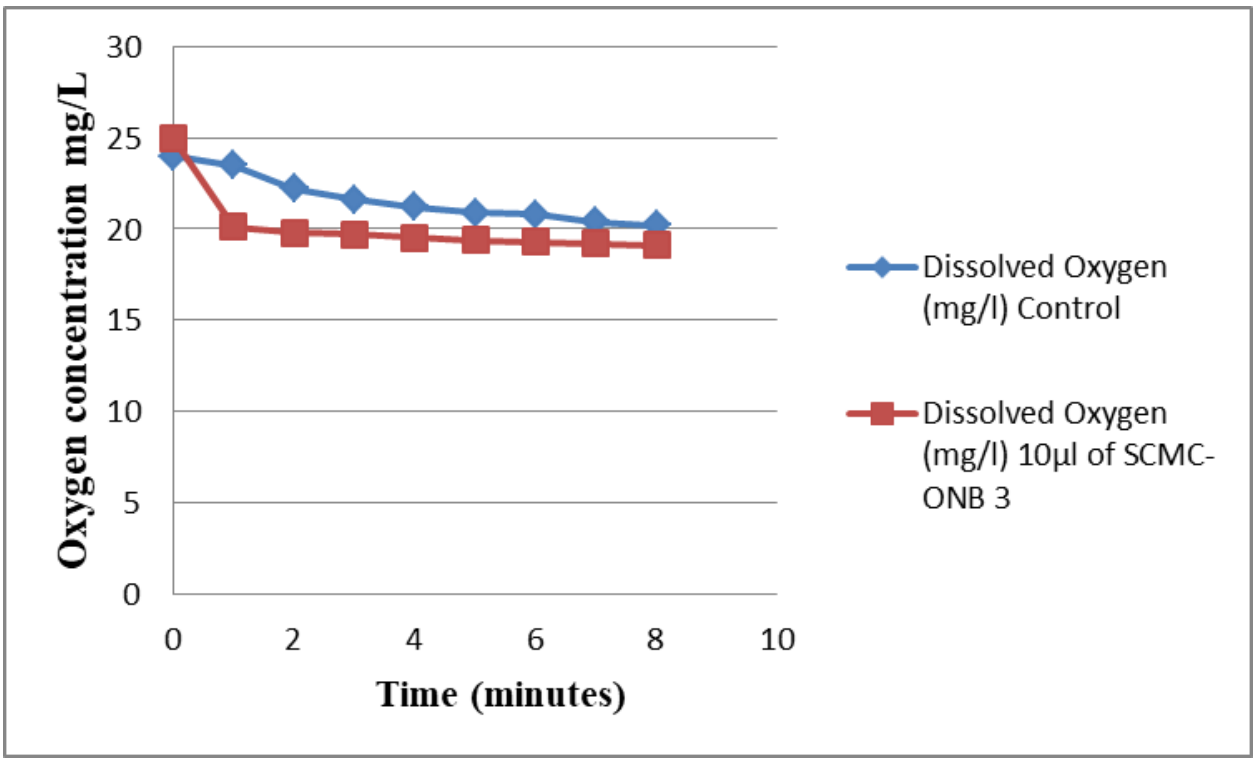

Figure 13:a) Graphical representation for dissolved oxygen content in 10µL SCMC- ONB 3

Table 6

b) Dissolved oxygen concentrations for 25µl of SCMC-ONB 3

Time (minutes)	Dissolved Oxygen (mg/l)	
	Control	**25µl of SCMC-ONB 3**
0	**23.0**	**26.0**
1	**21.3**	**21.8**
2	**20.8**	**20.9**
3	**20.7**	**20.5**
4	**20.6**	**20.3**
5	**20.5**	**20.1**
6	**20.4**	**19.8**
7	**20.3**	**19.7**
8	**20.2**	**19.6**

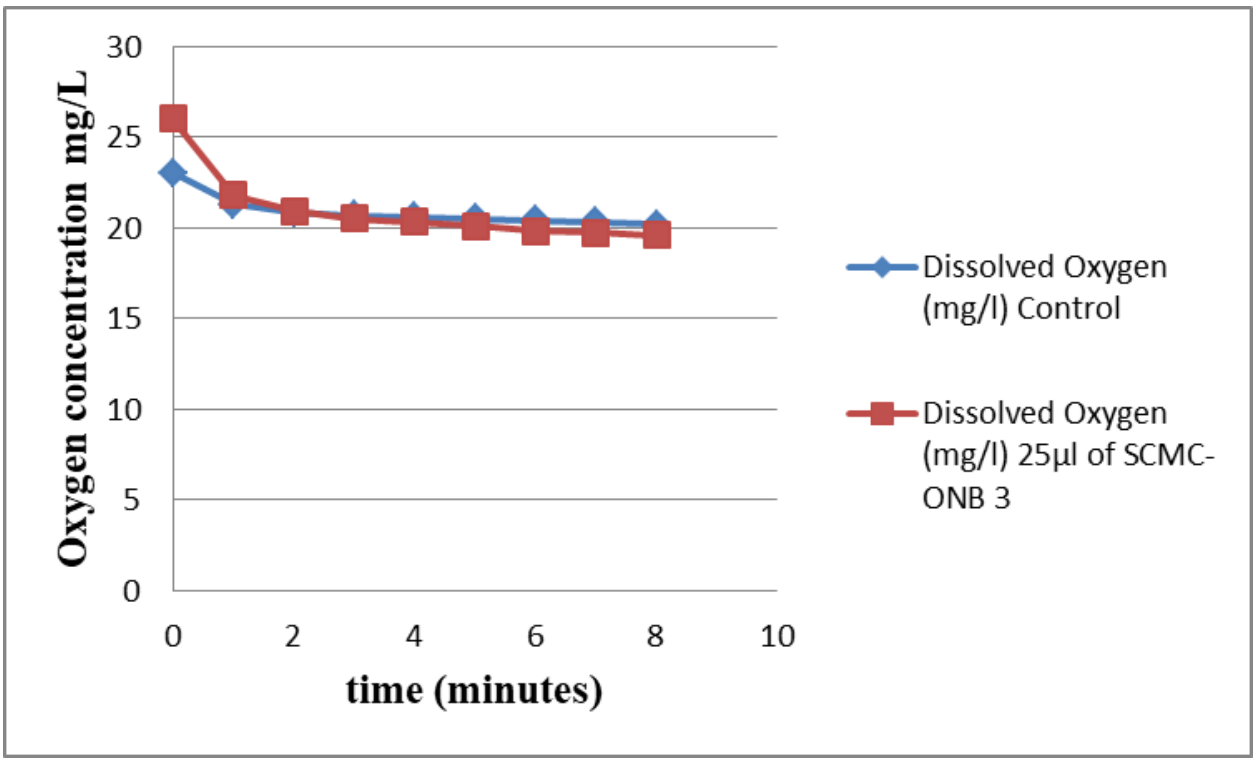

Figure 13: b) Graphical representation for dissolved oxygen content in 25µL SCMC-ONB 3

Table 6:

c) Dissolved oxygen concentrations for 50µl of SCMC-ONB 3

Time (minutes)	Dissolved Oxygen (mg/l)	
	Control	**50µl of SCMC-ONB 3**
0	**21.3**	**25.3**
1	**21.0**	**24.0**
2	**19.8**	**22.0**
3	**19.4**	**20.9**
4	**19.3**	**20.5**
5	**19.2**	**19.9**
6	**19.1**	**19.8**
7	**19.0**	**19.7**
8	**18.9**	**19.5**

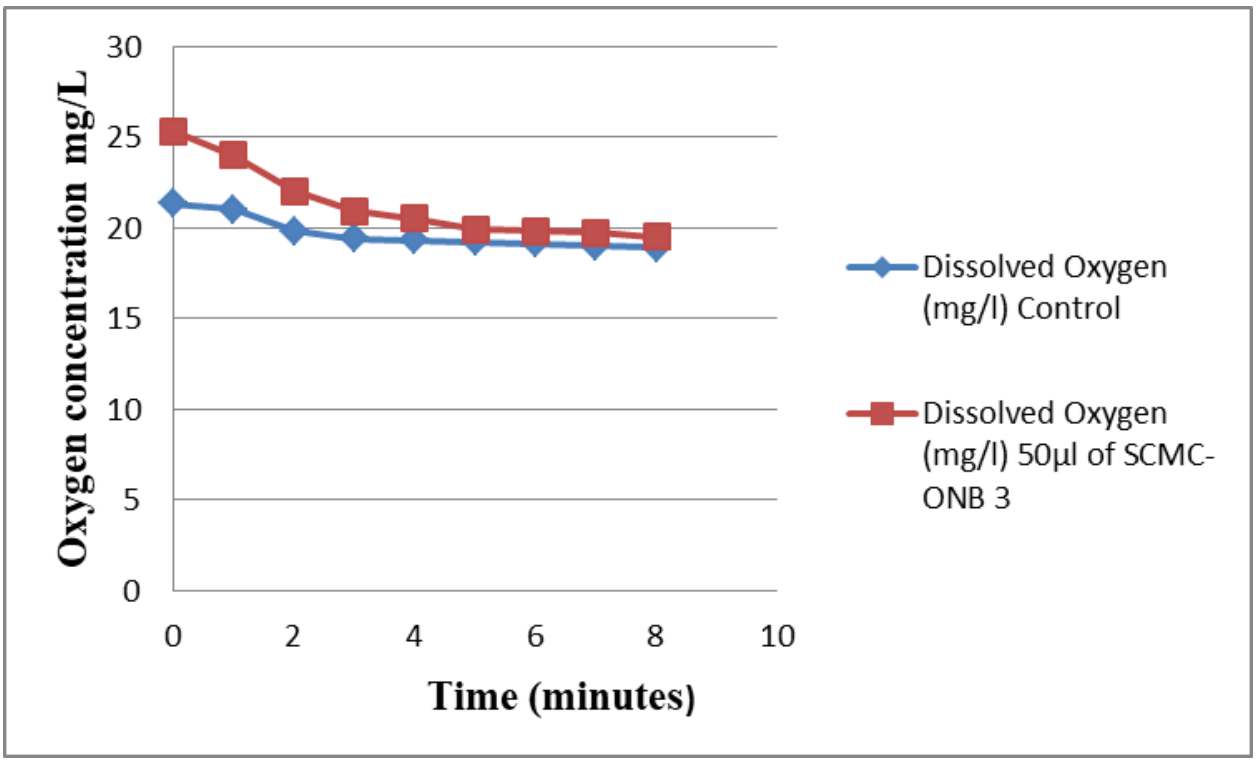

Figure 13: c) Graphical representation for dissolved oxygen content in 50µL SCMC-ONB **3**

Table 6

d) Dissolved oxygen concentrations at 100µl of SCMC-ONB 3

Time (minutes)	Dissolved Oxygen (mg/l)	
	Control	**100µl of SCMC-ONB 3**
0	**21.5**	**26.0**
1	**20.0**	**21.0**
2	**19.6**	**19.2**
3	**19.3**	**18.9**
4	**19.2**	**18.7**
5	**19.1**	**18.5**
6	**19.0**	**18.3**
7	**18.9**	**18.2**
8	**18.8**	**18.1**

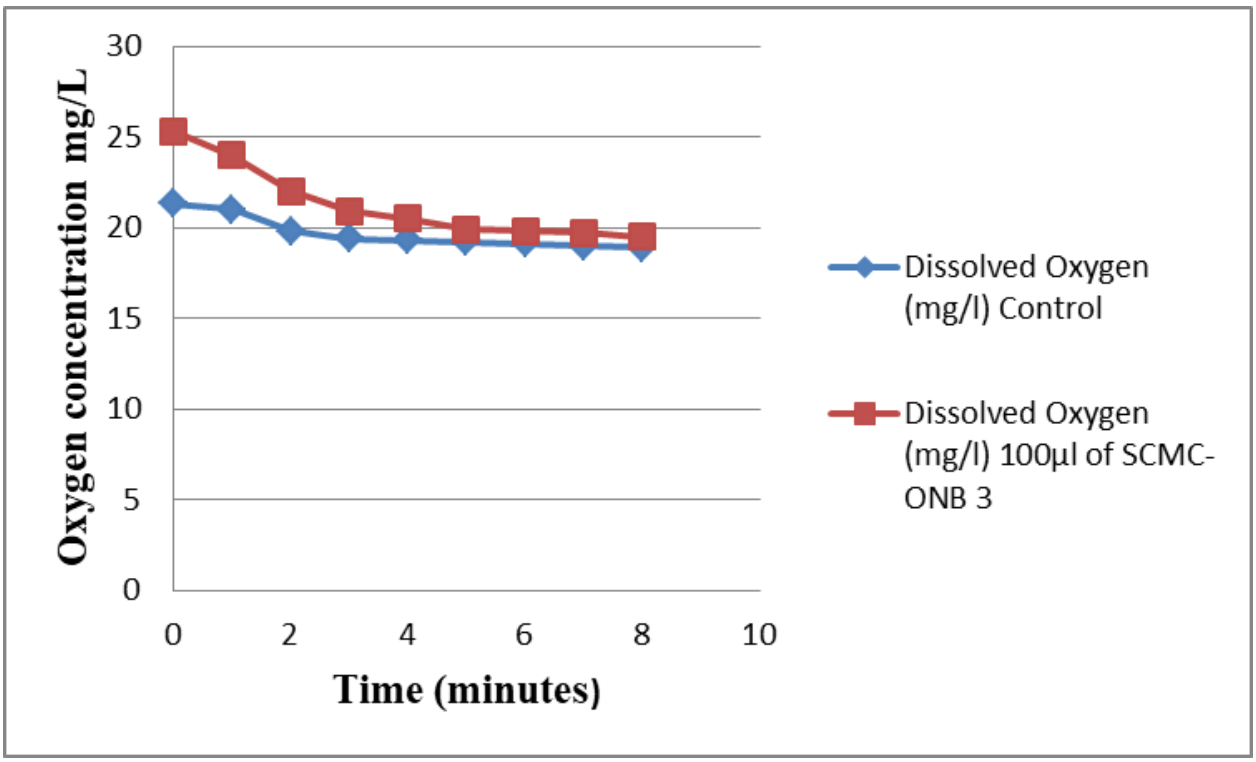

Figure 13:d)

Graphical representation for dissolved oxygen content in 100µL SCMC-ONB 3

Table 6: e)

S.No	Before adding SCMC-ONB dissolved oxygen (mg/L)	Volume of SCMC- ONB added (µL)	After adding SCMC- ONB 3 dissolved oxygen (mg/L)
1.	**20.0**	**10**	**19.1**
2.	**20.1**	**25**	**19.5**
3.	**18.9**	**50**	**19.5**
4.	**18.8**	**100**	**18.1**

Khan *et al.*, (2018) shows the oxygen release profile of ONBs in comparison with oxygenated DPBS and control. Nanobubbles rapidly increased oxygen saturation to

~4.9 mg/mL, as compared to ~3.2 mg/mL of oxygenated DPBS and 2.6 mg/mL of control sample from the starting point of 1.4 mg/mL after 1 min. Most of the nanobubbles released their oxygen in the initial 30 min of injection. The results indicate that ONBs approximately contained 500 µg/mL more oxygen as compared to oxygenated DPBS, demonstrating that approximately 50% volume of the suspension is oxygen gas. This showed that in a hypoxic environment, the diffusion of the oxygen gas out of bubbles was a rapid phenomenon. In the present study, no such increase in dissolved oxygen content was observed. Hence, we may conclude that SCMC-ONB does not release oxygen automatically under hypoxic conditions. From the EDX results, it was evident that oxygen concentration in the SCMC-ONB was high. However, diffusion of oxygen from the SCMC-ONB does not take place automatically.

Results of the paired-t test indicated that there is a non significant medium difference between control (M = 19.4 ,SD = 0.7) and SCMC- ONB3 added (M = 46.3 ,SD = 39.4), t(3) = 1.3, p = .273) samples.

H_0 hypothesis: Since the p-value > α, **H_0** can not be rejected. The dissolved oxygen population's average is considered to be equal to the (µL) population's average p-value equals 0.2732 It means that the chance of type I error, rejecting a correct **H_0** , is too high: 0.2732 (27.32%). The larger the p-value the more it supports **H_0**.

Test statistic T equals 1.3384, which is in the 95% region of acceptance: [-3.1824, 3.1824]. The 95% confidence interval of (µL) minus dissolved oxygen is: [-36.9265, 90.5265]

The observed effect size d is medium, 0.67. This indicates that the magnitude of the difference between the average of the differences and the expected average of the differences is medium.

Normality :The assumption was checked based on the Shapiro-Wilk Test. (α=0.05) It is assumed that (µL) minus dissolved oxygen does follow the normal distribution (p-value is 0.8447), or more accurately, you can't reject the normality assumption.

4.3 Assessment of hypoxia reversal

4.3.2 Induction of hypoxia

Cobalt has been widely used as a hypoxia mimic in cells. Cobalt chloride was used at different concentrations to obtain 50% cell viability to investigate the effect of acute hypoxia at cellular level.

Table 7

Different concentration of $CoCl_2$

S.No	Concentration of Cobalt Chloride (mM)	% Viability
1	0.05	49.00
2	0.25	41.00
3	0.50	38.00
4	0.75	34.00
5	1.00	39.70
6	2.00	40.90
7	3.00	41.40
8	4.00	37.50
9	5.00	25.70
10	6.00	22.43

49 % cell viability was obtained at 0.05 mM concentration of cobalt chloride, hence 0.05 mM $CoCl_2$ has been chosen for further assay.

4.3.3 Assessment of Hypoxia reversal by SCMC- ONB 3

Control = 10µL cells + 190µL PBS

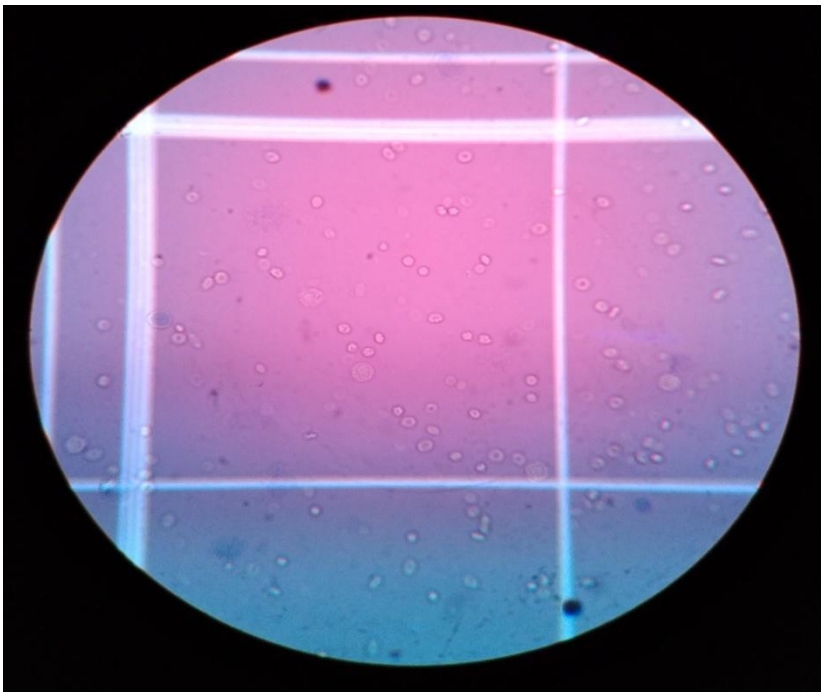

Figure 14: a) WBC cell count in control

Total number of cells = 372 X 10^4 per mL

$CoCl_2$ Control =10µL cells+189.75µL PBS+0.25µL$CoCl_2$

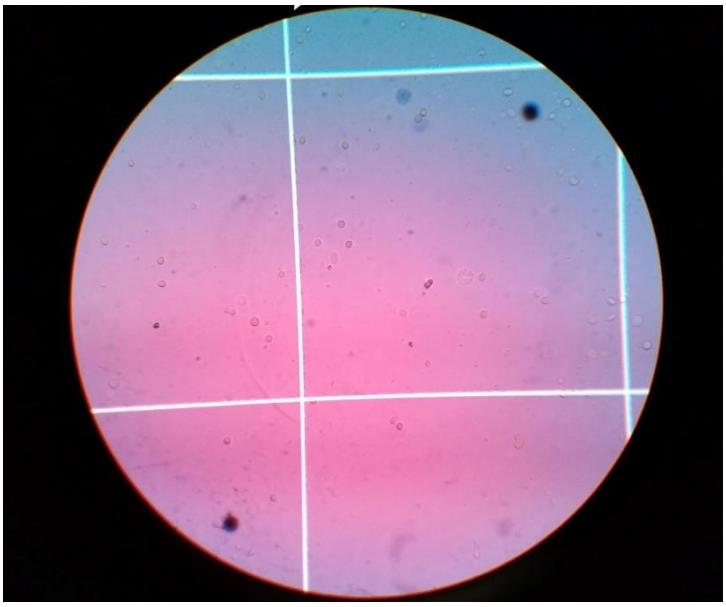

Figure 14: b) WBC cell count in $CoCl_2$ Control

SCMC-ONB treatment 1: 10µL cells+189.75µL PBS+0.25µL$CoCl_2$+50µL of SCMC- ONB 3

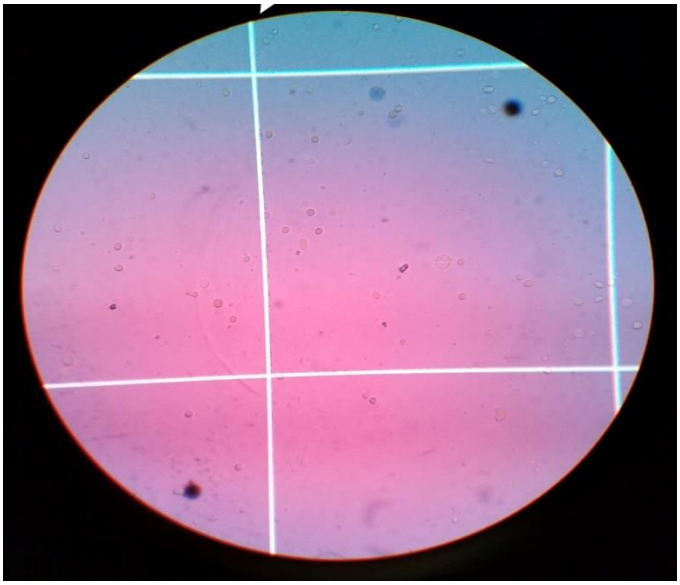

Figure 14 c) WBC cell count in SCMC-ONB treatment 1

SCMC-ONB treatment 2: 10µL cells+189.75µL PBS+0.25µL$CoCl_2$+100µL of SCMC-ONB 3

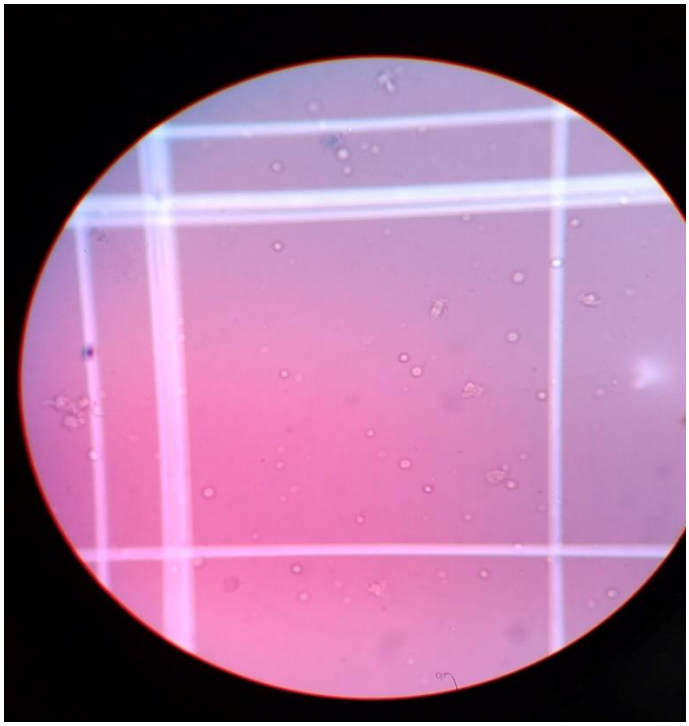

Figure: 14 d) WBC cell count in SCMC-ONB treatment 2

Table 8

Total Number of WBC count

S.No	Samples	Initial cell count x10^4 per mL	At 3 hours x10^4 per mL
1.	Control	372	346
2.	0.05mM $CoCl_2$	198	169
3.	50µL of SCMC- ONB 3	140	152
4.	100µL of SCMC- ONB 3	147	165

A chi-square test for independence compares two variables in a contingency table was performed to assess whether addition of SCMC-ONB influences cell viability in hypoxic cells. By comparing 0.05mM $CoCl_2$ induced hypoxic cells with 50µL of SCMC- ONB 3 treatment and 100µL of SCMC- ONB 3 treatment. The chi-square statistic is 4.3956, p- value is 0.22 indicating that the result is not significant at $p<.05$. There is no significant difference between $CoCl_2$ induced hypoxic cells and 50µL of SCMC- ONB 3 and 50µL of SCMC- ONB 3. From the results it is evident that SCMC-ONB does not improve cell viability.

Summary and Conclusion

5.0 SUMMARY AND CONCLUSION

Hypoxia induced damage is the root cause for several, outwardly unrelated diseases and disorders, including cancer, cardiovascular disease and neurodegenerative disorders. Reversing hypoxia when oxygenation by the lungs fails is a major challenge till date. The present study was undertaken with the objective of synthesizing oxygen nanobubbles and assessing their ability to reverse acute hypoxia in human peripheral blood lymphocytes . Human peripheral blood lymphocytes were chosen as a model system due to several advantages..

Before initiating the assay in peripheral blood lymphocytes, the dose of cobalt chloride to be used was optimized by assessing the cell viability. Varying concentrations of cobalt chloride were used 0.05mM, 0.25mM, 0.50mM, 0.75mM, 1mM, 2mM, 3mM, 4mM, 5mM and 6mM to induce hypoxia. From these, the optimum dose of cobalt chloride was found to be 50 μM respectively (50 % cell viability). Therefore, this dose was used in the subsequent assays.

Hypoxic stress was imposed in peripheral blood lymphocytes using cobalt chloride at 50μM final concentration. Acute hypoxia was achieved by incubating lymphocytes with cobalt chloride (50μM).. Viability was assessed by 0.4 % Trypan blue assay results showed that the exposure of cobalt chloride imposed an acute hypoxic stress in the lymphocytes. Using sodium carboxymethyl cellulose (SCMC) as a polymer shell, oxygen nanobubbles (ONB) are synthesized by ultrasonication, a stochastic method. SCMC-ONB 3 were characterized for analysis of morphology, elemental composition, surface area, functional group, crystallographic structure and dissolved oxygen content.

From the images from the FESEM, it is observed that SCMC-ONB 3 are not spherical in shape but of cylindrical shape. Inclusion of surfactants might have been beneficial to minimize the clumping of SCMC-ONBs. From EDX analysis, the percent weight of Oxygen of SCMC-ONB 3 is highest among all elements. Sodium and carbon are present in SCMC-ONB as part of the polymer, aluminum and chlorine act as a crosslinking agent and used to prevent size reduction of SCMC-ONB 3. Gold is not present in SCMC-ONB 3, but was used as a sputter coater for EDX analysis. So it shows up in the analysis.

SCMC-ONB 3 may contains hydroxyl group (OH), an alkene **(**C=C) or amine (NH) or imines (-C=N-), aliphatic bromo compounds (C-Br) or disulfides (S-S) and aliphatic iodo

compounds (C-I) at different frequencies where characterized by FTIR. Surface area of SCMC-ONB 3 was characterized by a 3D optical profiler. There is no change in width and distance of SCMC-ONB 1 and 2. Slight changes of width and distance from SCMC-ONB 3. As the time of sonication increased, the surface height of the nanobubble also increased, surface smoothness of the nanobubbles decreases and roughness of the nanobubble also decreased and became smooth or regular. Lower the sonication period the surface height was also varied, whereas for longer periods of sonication the surface was narrow and uniform for the nanobubbles and nanobubbles are more irregular. We can conclude that sonication time influences the surface smoothness and uniformity in the inverse way. XRD results that the strongest and sharpest diffraction peak at around 2θ was obtained are indexed as the reflection of crystalline structure in SCMC-ONB 3. Oxygen-loading capacities of SCMC- ONB 3 were found to be 19.1mg/L for 10 µL , 19.5mg/L for 25 µL, 19.5mg/L for 50µL and 18.1mg/L for 100µL, respectively by DO Meter. Results of the paired-t test indicated that there is a non significant medium difference between control ($M = 19.4$,$SD = 0.7$) and SCMC- ONB3 added ($M = 46.3$,$SD = 39.4$), $t(3) = 1.3$, $p = .273$) samples.

Peripheral blood lymphocytes are isolated by RBC lysis method, hypoxia induced by 0.05mM $CoCl_2$ at room temperature. Synthesized SCMC-ONB 3 were used in 2 concentrations : 50µL of SCMC-ONB added in one set of hypoxic cells and 100µL of SCMC-ONB added in another set of hypoxic cells. Cell viability was considered as the parameter for assessing hypoxia reversal. Cell viability was analyzed by 0.4 % Trypan blue assay.

A chi-square test for independence compares two variables in a contingency table to see if they are related. The result is not significant at $p<.05$. There is no significance between $CoCl_2$ induced hypoxic cells and 50µL of SCMC- ONB 3 and 100µL of SCMC- ONB3. From the results it is evident that SCMC-ONB does not improve cell viability.

In conclusion, SCMC-ONBs were prepared by sonication, but were not effective in reversing hypoxia in isolated peripheral isolated lymphocytes.

Bibliography

BIBLIOGRAPHY

Agrawal, S., & Rathore, P. (2014). Nanotechnology pros and cons to agriculture: a review. *Int J Curr Microbiol App Sci*, *3*(3), 43-55.

Ali, S., Khan, I., Khan, S. A., Sohail, M., Ahmed, R., ur Rehman, A., ... & Morsy, M. A. (2017). Electrocatalytic performance of Ni@ Pt core–shell nanoparticles supported on carbon nanotubes for methanol oxidation reaction. *Journal of Electroanalytical Chemistry*, *795*, 17-25.

Astefanei, A., Núñez, O., & Galceran, M. T. (2015). Characterisation and determination of fullerenes: a critical review. *Analytica chimica acta*, *882*, 1-21.

Avelar-Freitas, B. A., Almeida, V. G. Pinto, M. C, Mourão, F. A. Massensini, A. R., Martins-Filho, O. A., Rocha-Vieira, E., & Brito-Melo, G. , E. (2014). Trypan blue exclusion assay by flow cytometry. *Brazilian journal of medical and biological research = Revista brasileira de pesquisas medicas e biologicas*, *47*(4), 307–315. https://doi.org/10.1590/1414-431X20143437

Bae, S., Jeong, H. J., Cha, H. J., Kim, K., Choi, Y. M., An, I. S., Koh, H. J., Lim, D. J., Lee, S. J., & An, S. (2012). The hypoxia-mimetic agent cobalt chloride induces cell cycle arrest and alters gene expression in U266 multiple myeloma cells. *International journal of molecular medicine*, *30*(5), 1180–1186. https://doi.org/10.3892/ijmm.2012.1115

Baldi, S., Aquilani, R., Pinna, G. D., Poggi, P., De Martini, A., & Bruschi, C. (2010). Fat-free mass change after nutritional rehabilitation in weight losing COPD: role of insulin, C-reactive protein and tissue hypoxia. *International journal of chronic obstructive pulmonary disease*, *5*, 29–39. https://doi.org/10.2147/copd.s7739

Bhandari, P. N., Cui, Y., Elzey, B. D., Goergen, C. J., Long, C. M., & Irudayaraj, J. (2017). Oxygen nanobubbles revert hypoxia by methylation programming. *Scientific reports*, *7*(1), 9268. https://doi.org/10.1038/s41598-017-08988-7

Boverhof, D. R., Bramante, C. M., Butala, J. H., Clancy, S. F., Lafranconi, M., West, J., & Gordon, S. C. (2015). Comparative assessment of nanomaterial definitions and safety evaluation considerations. *Regulatory toxicology and pharmacology : RTP*, *73*(1), 137–150. https://doi.org/10.1016/j.yrtph.2015.06.001

Brown, J. M., & Giaccia, A. J. (1998). The unique physiology of solid tumors: opportunities (and problems) for cancer therapy. *Cancer research*, *58*(7), 1408–1416.

Burtscher, M., Gatterer, H., Burtscher, J., & Mairbäurl, H. (2018). Extreme Terrestrial Environments: Life in Thermal Stress and Hypoxia. A Narrative Review. *Frontiers in physiology*, *9*, 572. https://doi.org/10.3389/fphys.2018.00572

C Thomas, S., Kumar Mishra, P., & Talegaonkar, S. (2015). Ceramic nanoparticles: fabrication methods and applications in drug delivery. *Current pharmaceutical design*, *21*(42), 6165-6188.
Cao, Y. C., Jin, R., Nam, J. M., Thaxton, C. S., & Mirkin, C. A. (2003). Raman dye-labeled nanoparticle probes for proteins. *Journal of the American Chemical Society*, *125*(48), 14676–14677. https://doi.org/10.1021/ja0366235

Cavalli, R., Bisazza, A., & Lembo, D. (2013). Micro- and nanobubbles: a versatile non-viral platform for gene delivery. *International journal of pharmaceutics*, *456*(2), 437–445. https://doi.org/10.1016/j.ijpharm.2013.08.041

Cavalli, R., Soster, M., & Argenziano, M. (2016). Nanobubbles: a promising efficient tool for therapeutic delivery. *Therapeutic delivery*, *7*(2), 117–138. https://doi.org/10.4155/tde.15.92

Chen, H., Zhou, K., & Zhao, G. (2018). Gold nanoparticles: From synthesis, properties to their potential application as colorimetric sensors in food safety screening. *Trends in food science & technology*, *78*, 83-94.

Choi, J.; Lee, E.K.; Choo, J.; Yuh, J.; Hong, J.W. Micro 3d cell culture systems for cellular behavior studies: Culture matrices, devices, substrates, and in-situ sensing methods. Biotechnol. J. 2015, 10, 1682–1688.

Chung, Jae; Edewi, Oghosa; Foppen, Jan; Gerner, Gabriel; Krebs, Rolf; Lens, Piet (2017). *Removal of Escherichia coli by Intermittent Operation of Saturated Sand Columns Supplemented with Hydrochar Derived from Sewage Sludge. Applied Sciences, 7(8), 839–*. doi:10.3390/app7080839

Coppel, J., Hennis, P., Gilbert-Kawai, E., & Grocott, M. P. (2015). The physiological effects of hypobaric hypoxia versus normobaric hypoxia: a systematic review of crossover trials. *Extreme physiology & medicine*, *4*, 2. https://doi.org/10.1186/s13728-014-0021-6

Dagur, P. K., & McCoy, J. P., Jr (2015). Collection, Storage, and Preparation of Human Blood Cells. *Current protocols in cytometry*, *73*, 5.1.1–5.1.16. https://doi.org/10.1002/0471142956.cy0501s73

Diaz R. J. (2001). Overview of hypoxia around the world. *Journal of environmental quality*, *30*(2), 275–281. https://doi.org/10.2134/jeq2001.302275x

Dreaden, E. C., Alkilany, A. M., Huang, X., Murphy, C. J., & El-Sayed, M. A. (2012). The golden age: gold nanoparticles for biomedicine. *Chemical Society Reviews*, *41*(7), 2740-2779.

Elahi, N., Kamali, M., & Baghersad, M. H. (2018). Recent biomedical applications of gold nanoparticles: A review. *Talanta*, *184*, 537-556.

Fadlelmoula, A., Pinho, D., Carvalho, V. H., Catarino, S. O., & Minas, G. (2022). Fourier Transform Infrared (FTIR) Spectroscopy to Analyse Human Blood over the Last 20 Years: A Review towards Lab-on-a-Chip Devices. *Micromachines*, *13*(2), 187. https://doi.org/10.3390/mi13020187

Garvey, J. F., Taylor, C. T., & McNicholas, W. T. (2009). Cardiovascular disease in obstructive sleep apnoea syndrome: the role of intermittent hypoxia and inflammation. *The European respiratory journal*, *33*(5), 1195–1205. https://doi.org/10.1183/09031936.00111208

Grocott, M., Montgomery, H., & Vercueil, A. (2007). High-altitude physiology and pathophysiology: implications and relevance for intensive care medicine. *Critical care (London, England)*, *11*(1), 203. https://doi.org/10.1186/cc5142

Gros, A., Parkhurst, M. R., Tran, E., Pasetto, A., Robbins, P. F., Ilyas, S., Prickett, T. D., Gartner, J. J., Crystal, J. S., Roberts, I. M., Trebska-McGowan, K., Wunderlich, J. R., Yang, J. C., & Rosenberg, S. A. (2016). Prospective identification of neoantigen-specific lymphocytes in the peripheral blood of melanoma patients. *Nature medicine*, *22*(4), 433–438. https://doi.org/10.1038/nm.4051

Gujrati, M., Malamas, A., Shin, T., Jin, E., Sun, Y., & Lu, Z. R. (2014). Multifunctional cationic lipid-based nanoparticles facilitate endosomal escape and reduction-triggered cytosolic siRNA release. *Molecular pharmaceutics*, *11*(8), 2734-2744.

Hayday, A., Theodoridis, E., Ramsburg, E., & Shires, J. (2001). Intraepithelial lymphocytes: exploring the Third Way in immunology. *Nature immunology*, *2*(11), 997–1003. https://doi.org/10.1038/ni1101-997

Hiwa M. Ahmed, Arpita Roy, Muhammad Wahab, Mohammed Ahmed, Gashaw Othman-Qadir, Basem H. Elesawy, Mayeen Uddin Khandaker, Mohammad Nazmul Islam, Talha Bin Emran, "Applications of Nanomaterials in Agrifood and Pharmaceutical Industry", *Journal of Nanomaterials*, vol. 2021, Article ID 1472096, 10 pages, 2021. https://doi.org/10.1155/2021/1472096

Holland, H. D. (2002). *Volcanic gases, black smokers, and the great oxidation event. Geochimica et Cosmochimica Acta, 66(21), 3811–3826.* doi:10.1016/s0016-7037(02)00950-x

Iijima, M., Gombodorj, N., Tachibana, Y., Tachibana, K., Yokobori, T., Honma, K., Nakano, T., Asao, T., Kuwahara, R., Aoyama, K., Yasuda, H., Kelly, M., Kuwano, H., & Yamanouchi, D. (2018). Development of single nanometer-sized ultrafine oxygen bubbles to overcome the hypoxia-induced resistance to radiation therapy via the suppression of hypoxia-inducible factor-1α. *International journal of oncology*, *52*(3), 679–686. https://doi.org/10.3892/ijo.2018.4248

Iyer, N. V., Leung, S. W., & Semenza, G. L. (1998). The human hypoxia-inducible factor 1alpha gene: HIF1A structure and evolutionary conservation. *Genomics*, *52*(2), 159–165. https://doi.org/10.1006/geno.1998.5416

Kapłonek, W., Mikolajczyk, T., Pimenov, D. Y., Gupta, M. K., Mia, M., Sharma, S., Patra, K., & Sutowska, M. (2020). High-Accuracy 3D Optical Profilometry for Analysis of Surface Condition of Modern Circulated Coins. *Materials (Basel, Switzerland)*, *13*(23), 5371. https://doi.org/10.3390/ma13235371

Kayalvizhi, C., Anand, S., Durga, R., Ebinezer, B. S., & Sundararajan, R. S. (2020). Structural, vibrational and optical studies on semiorganic crystals of boric acid potassium acetate. *Heliyon*, *6*(1), e03133. https://doi.org/10.1016/j.heliyon.2019.e03133

Keller, T.F.; Volkov, S.; Navickas, E.; Kulkarni, S.; Vonk, V.; Fleig, J.; Stierle, A. (2019). *Nano-scale oxide formation inside electrochemically-formed Pt blisters at a solid electrolyte interface. Solid State Ionics, 330(), 17–23.* doi:10.1016/j.ssi.2018.11.009

Khan, I., Abdalla, A., & Qurashi, A. (2017). Synthesis of hierarchical WO3 and Bi2O3/WO3 nanocomposite for solar-driven water splitting applications. *international journal of hydrogen energy*, *42*(5), 3431-3439.

Khan, Ibrahim; Saeed, Khalid; Khan, Idrees (2017). Nanoparticles: Properties, Applications and Toxicities. Arabian Journal of Chemistry, (), S1878535217300990–. doi:10.1016/j.arabjc.2017.05.011

Khan, M. S., Hwang, J., Seo, Y., Shin, K., Lee, K., Park, C., Choi, Y., Hong, J. W., & Choi, J. (2018). Engineering oxygen nanobubbles for the effective reversal of hypoxia. *Artificial cells, nanomedicine, and biotechnology*, *46*(sup3), S318–S327. https://doi.org/10.1080/21691401.2018.1492420

Kheir, J. N., Polizzotti, B. D., Thomson, L. M., O'Connell, D. W., Black, K. J., Lee, R. W., Wilking, J. N., Graham, A. C., Bell, D. C., & McGowan, F. X. (2013). Bulk manufacture of concentrated oxygen gas-filled microparticles for intravenous oxygen delivery. *Advanced healthcare materials*, *2*(8), 1131–1141. https://doi.org/10.1002/adhm.201200350

Kim, E. J., Lee, J. E., Yoon, S., Lee, D. J., Mai, H. N., Ida-Yonemochi, H., Choi, J., & Jung, H. S. (2021). Hypoxia-Responsive Oxygen Nanobubbles for Tissues-Targeted Delivery in Developing Tooth Germs. *Frontiers in cell and developmental biology*, *9*, 626224. https://doi.org/10.3389/fcell.2021.626224

LeBleu, V. S., Taduri, G., O'Connell, J., Teng, Y., Cooke, V. G., Woda, C., Sugimoto, H., & Kalluri, R. (2013). Origin and function of myofibroblasts in kidney fibrosis. *Nature medicine*, *19*(8), 1047–1053. https://doi.org/10.1038/nm.3218

Lee, M., Lee, E. Y., Lee, D., & Park, B. J. (2015). Stabilization and fabrication of microbubbles: applications for medical purposes and functional materials. *Soft matter*, *11*(11), 2067–2079. https://doi.org/10.1039/c5sm00113g.

LEWIS, R. B., & HAYMAKER, W. (1948). High altitude hypoxia; observations at autopsy in 75 cases and an analysis of the causes of the hypoxia. *The Journal of aviation medicine*, *19*(5), 306–336.

Liu, X., Xu, C., & Duan, Z. (2017). A Simple Red Blood Cell Lysis Method for the Establishment of B Lymphoblastoid Cell Lines. *Journal of visualized experiments : JoVE*, (119), 55191. https://doi.org/10.3791/55191

Loreti, E., van Veen, H., & Perata, P. (2016). Plant responses to flooding stress. *Current opinion in plant biology*, *33*, 64–71. https://doi.org/10.1016/j.pbi.2016.06.005

Lovisa, S., Zeisberg, M., & Kalluri, R. (2016). Partial Epithelial-to-Mesenchymal Transition and Other New Mechanisms of Kidney Fibrosis. *Trends in endocrinology and metabolism: TEM*, *27*(10), 681–695. https://doi.org/10.1016/j.tem.2016.06.004

Lyons, T. W., Reinhard, C. T., & Planavsky, N. J. (2014). The rise of oxygen in Earth's early ocean and atmosphere. *Nature*, *506*(7488), 307–315. https://doi.org/10.1038/nature13068

Mansha, M., Khan, I., Ullah, N., & Qurashi, A. (2017). Synthesis, characterization and visible-light-driven photoelectrochemical hydrogen evolution reaction of carbazole-containing conjugated polymers. *International Journal of Hydrogen Energy*, *42*(16), 10952-10961.

Martin, D., McKenna, H., & Livina, V. (2017). The human physiological impact of global deoxygenation. *The journal of physiological sciences : JPS*, *67*(1), 97–106. https://doi.org/10.1007/s12576-016-0501-0

Mashaghi, S., Jadidi, T., Koenderink, G., & Mashaghi, A. (2013). Lipid nanotechnology. *International journal of molecular sciences*, *14*(2), 4242-4282.

Matear, R. J., & Hirst, A. C. (2003). Long-term changes in dissolved oxygen concentrations in the ocean caused by protracted global warming. *Global Biogeochemical Cycles*, *17*(4).

Mayeen, Anshida (2018). Characterization of Nanomaterials || Morphological Characterization of Nanomaterials. , (), 335–364. doi:10.1016/B978-0-08-101973-3.00012-2

McEwan, C., Owen, J., Stride, E., Fowley, C., Nesbitt, H., Cochrane, D., Coussios, C. C., Borden, M., Nomikou, N., McHale, A. P., & Callan, J. F. (2015). Oxygen carrying microbubbles for enhanced sonodynamic therapy of hypoxic tumours. *Journal of*

controlled release : official journal of the Controlled Release Society, *203*, 51–56. https://doi.org/10.1016/j.jconrel.2015.02.004

Meletis, Chris & Wilkesa, Kimberly. (2019). The Crucial Role of Oxygen for Health. Journal of Restorative Medicine. 8. 10.14200/jrm.2019.0106.

Monge-C, C., Arregui, A., & León-Velarde, F. (1992). Pathophysiology and epidemiology of chronic mountain sickness. *International journal of sports medicine*, *13 Suppl 1*, S79–S81. https://doi.org/10.1055/s-2007-1024603

Moore, L. G., Niermeyer, S., & Zamudio, S. (1998). Human adaptation to high altitude: regional and life-cycle perspectives. *American journal of physical anthropology*, *Suppl 27*, 25–64. https://doi.org/10.1002/(sici)1096-8644(1998)107:27+<25::aid-ajpa3>3.0.co;2-l

Nadeem Baig;Irshad Kammakakam;Wail Falath; (2021). *Nanomaterials: a review of synthesis methods, properties, recent progress, and challenges . Materials Advances, (), –* . doi:10.1039/d0ma00807a

Naderi, M. R., & Danesh-Shahraki, A. (2013). Nanofertilizers and their roles in sustainable agriculture. *International Journal of Agriculture and Crop Sciences*, *5*(19), 2229.

Nair, R., Varghese, S. H., Nair, B. G., Maekawa, T., Yoshida, Y., & Kumar, D. S. (2010). Nanoparticulate material delivery to plants. *Plant science*, *179*(3), 154-163.

Puri, A., Loomis, K., Smith, B., Lee, J. H., Yavlovich, A., Heldman, E., & Blumenthal, R. (2009). Lipid-based nanoparticles as pharmaceutical drug carriers: from concepts to clinic. *Critical Reviews™ in Therapeutic Drug Carrier Systems*, *26*(6).

Qi, K., & Xin, J. H. (2010). Room-temperature synthesis of single-phase anatase TiO2 by aging and its self-cleaning properties. ACS applied materials & interfaces, 2(12), 3479–3485. https://doi.org/10.1021/am1005892

Rao, J. P., & Geckeler, K. E. (2011). Polymer nanoparticles: preparation techniques and size-control parameters. *Progress in polymer science*, *36*(7), 887-913.

Rawat, M. K., Jain, A., & Singh, S. (2011). Studies on binary lipid matrix based solid lipid nanoparticles of repaglinide: in vitro and in vivo evaluation. *Journal of pharmaceutical sciences*, *100*(6), 2366-2378.

Rettew, R. E., Allam, N. K., & Alamgir, F. M. (2011). Interface architecture determined electrocatalytic activity of Pt on vertically oriented TiO(2) nanotubes. *ACS applied materials & interfaces*, *3*(2), 147–151. https://doi.org/10.1021/am1012563

Rinderknecht, H.; Ehnert, S.; Braun, B.; Histing, T.; Nussler, A.K.; Linnemann, C. The Art of Inducing Hypoxia. Oxygen 2021, 1, 46–61. https://doi.org/10.3390/ oxygen1010006

Roca, A. G., Gutiérrez, L., Gavilán, H., Brollo, M. E. F., Veintemillas-Verdaguer, S., & del Puerto Morales, M. (2019). Design strategies for shape-controlled magnetic iron oxide nanoparticles. *Advanced drug delivery reviews*, *138*, 68-104.

Rocha S. (2007). Gene regulation under low oxygen: holding your breath for transcription. *Trends in biochemical sciences*, *32*(8), 389–397. https://doi.org/10.1016/j.tibs.2007.06.005

Ronaldson, P. T., & Davis, T. P. (2013). Targeted drug delivery to treat pain and cerebral hypoxia. *Pharmacological reviews*, *65*(1), 291–314. https://doi.org/10.1124/pr.112.005991

Sadjadi, Samahe; Heravi, Majid M.; Daraie, Mansoureh (2017). Cyclodextrin nanosponges: a potential catalyst and catalyst support for synthesis of xanthenes. Research on Chemical Intermediates, 43(2), 843–857. doi:10.1007/s11164-016-2668-7

Saleh, Tawfik A. (2020). *Nanomaterials: Classification, properties, and environmental toxicities. Environmental Technology & Innovation, (), 101067–*. doi:10.1016/j.eti.2020.101067

Schito, L., & Semenza, G. L. (2016). Hypoxia-Inducible Factors: Master Regulators of Cancer Progression. *Trends in cancer*, *2*(12), 758–770. https://doi.org/10.1016/j.trecan.2016.10.016

Sendoel, A., & Hengartner, M. O. (2014). Apoptotic cell death under hypoxia. *Physiology (Bethesda, Md.)*, *29*(3), 168–176. https://doi.org/10.1152/physiol.00016.2013

Shin, W. K., Cho, J., Kannan, A. G., Lee, Y. S., & Kim, D. W. (2016). Cross-linked composite gel polymer electrolyte using mesoporous methacrylate-functionalized SiO2 nanoparticles for lithium-ion polymer batteries. *Scientific reports*, *6*(1), 1-10.

Sigmund, W., Yuh, J., Park, H., Maneeratana, V., Pyrgiotakis, G., Daga, A., ... & Nino, J. C. (2006). Processing and structure relationships in electrospinning of ceramic fiber systems. *Journal of the American Ceramic Society*, *89*(2), 395-407.

Sluimer, J. C., & Daemen, M. J. (2009). Novel concepts in atherogenesis: angiogenesis and hypoxia in atherosclerosis. *The Journal of pathology*, *218*(1), 7–29. https://doi.org/10.1002/path.2518

Su, H., Jing, L., Shi, K. *et al.* Synthesis of large surface area $LaFeO_3$ nanoparticles by SBA-16 template method as high active visible photocatalysts. *J Nanopart Res* **12,** 967–974 (2010). https://doi.org/10.1007/s11051-009-9647-5

Sun, J., Yin, M., Zhu, S., Liu, L., Zhu, Y., Wang, Z., Xu, R. X., & Chang, S. (2016). Ultrasound-mediated destruction of oxygen and paclitaxel loaded lipid microbubbles for combination therapy in hypoxic ovarian cancer cells. *Ultrasonics sonochemistry*, *28*, 319–326. https://doi.org/10.1016/j.ultsonch.2015.08.009

Sun, S., Murray, C. B., Weller, D., Folks, L., & Moser, A. (2000). Monodisperse FePt nanoparticles and ferromagnetic FePt nanocrystal superlattices. *science*, *287*(5460), 1989-1992.

Trayhurn, P., Wang, B., & Wood, I. S. (2008). Hypoxia and the endocrine and signalling role of white adipose tissue. *Archives of physiology and biochemistry*, *114*(4), 267–276. https://doi.org/10.1080/13813450802306602

Tretter, V., Zach, M. L., Böhme, S., Ullrich, R., Markstaller, K., & Klein, K. U. (2020). Investigating Disturbances of Oxygen Homeostasis: From Cellular Mechanisms to the Clinical Practice. *Frontiers in physiology*, *11*, 947. https://doi.org/10.3389/fphys.2020.00947

Urbansky, A., Ohlsson, P., Lenshof, A. *et al.* Rapid and effective enrichment of mononuclear cells from blood using acoustophoresis. *Sci Rep* **7,** 17161 (2017). https://doi.org/10.1038/s41598-017-17200-9

Vivier, E., Tomasello, E., Baratin, M., Walzer, T., & Ugolini, S. (2008). Functions of natural killer cells. *Nature immunology*, *9*(5), 503–510. https://doi.org/10.1038/ni1582

Wagner, B. A., Venkataraman, S., & Buettner, G. R. (2011). The rate of oxygen utilization by cells. *Free radical biology & medicine*, *51*(3), 700–712. https://doi.org/10.1016/j.freeradbiomed.2011.05.024

Wang Y.; Bhushan B. Boundary slip and nanobubble study in micro/nanofluidics using atomic force microscopy. Soft Matter 2010, 6, 29–66. 10.1039/b917017k.

Wang, X., & Zhang, Y. (2009). Degradation of alachlor in aqueous solution by using hydrodynamic cavitation. *Journal of hazardous materials*, *161*(1), 202–207. https://doi.org/10.1016/j.jhazmat.2008.03.073

Wei, Y., Jiao, Y., An, D., Li, D., Li, W., & Wei, Q. (2019). Review of Dissolved Oxygen Detection Technology: From Laboratory Analysis to Online Intelligent Detection. *Sensors (Basel, Switzerland)*, *19*(18), 3995. https://doi.org/10.3390/s19183995

Weits, D. A., van Dongen, J. T., & Licausi, F. (2021). Molecular oxygen as a signaling component in plant development. *The New phytologist*, *229*(1), 24–35. https://doi.org/10.1111/nph.16424

West J. B. (2000). Human limits for hypoxia. The physiological challenge of climbing Mt. Everest. *Annals of the New York Academy of Sciences*, *899*, 15–27. https://doi.org/10.1111/j.1749-6632.2000.tb06173.x

Wood, K. J., & Sakaguchi, S. (2003). Regulatory T cells in transplantation tolerance. *Nature reviews. Immunology*, *3*(3), 199–210. https://doi.org/10.1038/nri1027

Wu, D., & Yotnda, P. (2011). Induction and testing of hypoxia in cell culture. *Journal of visualized experiments : JoVE*, (54), 2899. https://doi.org/10.3791/2899

Xu R. X. (2011). Multifunctional microbubbles and nanobubbles for photoacoustic imaging. *Contrast media & molecular imaging*, *6*(5), 401–411. https://doi.org/10.1002/cmmi.442.

Zhang, H., Lyu, T., Bi, L., Tempero, G., Hamilton, D. P., & Pan, G. (2018). Combating hypoxia/anoxia at sediment-water interfaces: A preliminary study of oxygen nanobubble modified clay materials. *The Science of the total environment*, *637-638*, 550–560. https://doi.org/10.1016/j.scitotenv.2018.04.284

Appendix

Appendix I

Synthesis of Sodium Carboxymethyl Cellulose Oxygen Nanobubbles (SCMC- ONB)

(Bhandari *et al.*, 2017)

Principle

Sodium carboxymethyl cellulose is a linear polymeric derivative of natural cellulose. The shells made of CMC are thicker, thus providing a stronger barrier against dissolution of the entrapped oxygen and improving oxygen delivery under hypoxic conditions.

Reagents

1. 0.1% Sodium Carboxymethyl Cellulose (SCMC)
2. Oxygen gas
3. 1% Aluminum chloride ($AlCl_3$)
4. 0.1% Ammonium hydroxide (NH_4OH)

Procedure

Sodium carboxymethyl cellulose was dissolved in nanopure water to form a 0.1% (w/v) gel and homogenized and saturated with oxygen gas. The oxygen inlet was connected with an air nozzle and a 20 nm membrane filter to help generate oxygen nanobubbles. The carboxymethyl cellulose solution was sonicated simultaneously with a probe, since ultrasonic energy helps sonic compression of oxygen microbubbles to produce oxygen nanobubbles in the solution. Finally, 1% aluminum chloride ($AlCl_3$) cross-linking agent was added to form the encapsulation structure under continuous ultrasonication. Aluminum chloride is a trivalent cross linker and helps decrease the gas release rate compared to bivalent cross linkers. Aluminum chloride also serves as a strong electrolyte and increases the electrostatic repulsive force to balance out the size reduction forces of the nanobubble, thus stabilizing the nanobubble. The pH of the resulting nanobubble suspension was subsequently neutralized to a pH of 7 using 0.1% ammonium hydroxide (NH_4OH) solution added drop wise.

Appendix II

Field Emission Scanning Electron Microscope (FESEM)

(Chung *et al.*, 2017)

Principle

FESEM is a microscope that works with electron particles with a negative charge instead of light. These electrons are liberated by a field emission source. The object is scanned by electrons according to a zig-zag pattern.

Procedure

The surface morphology of the sodium carboxy methyl cellulose oxygen nanobubbles was investigated by performing a Scanning Electron Microscopy (SEM) analysis using a Quanta 250 FEG. Sample solution was placed with an adhesive side of carbon conductive tape. This is because carbon has a low atomic number and the peak of the X-ray graph of carbon doesn't interfere with other peaks of other elements and sputtered with gold, to prevent charge build upon sample surface and images were viewed under microscopy. Electrons generated from an electron gun enter on the surface of a sample and in elastic interaction with atoms in the specimen, produces a variety of signals that contains the information about the surface morphology and composition. The main operating parameters were: 20 kV as gun voltage and a working distance of about 10.3 mm. Sample was examined at different magnifications (2400X, 5000X, 10000X, 20000X). Pictures were taken in the same position at the approximate centre of the main sample.

Appendix III

Energy-dispersive X-ray spectroscopy (EDX)

(Chung *et al*., 2017)

Principle

The major operating principle that allows EDX to function is the capacity of high energy electromagnetic radiation (X-rays) to eject 'core' electrons (electrons that are not in the outermost shell) from an atom. This principle is known as Moseley's Law, which determines that there was a direct correlation between the frequency of light released and the atomic number of the atom. This helps in assessing the elemental composition of the sample.

Procedure

Sodium carboxymethyl cellulose oxygen nanobubbles samples were analyzed in order to analyze elemental composition using QUANTAX EDS SOP BRUKER. For reliable quantitative

measurements, the sample should be shaved as thin as possible. Sample solution was placed with an adhesive side of carbon conductive tape, this is because carbon has a low atomic number and the peak of the X-ray graph of carbon doesn't interfere with other peaks of other elements and sputtered with gold, to prevent charge build upon sample surface and measurements were taken under EDX analyzer. It generates data made up of spectra with peaks corresponding to the various components that are present in the sample.

Appendix IV

Fourier Transform Infrared Spectroscopy (FTIR)

(Fadlelmoula *et al*., 2022)

Principle

In FTIR analyses, Infrared light from the light source passes through a Michelson interferometer along the optical path. An FTIR spectrum arises from interferograms being 'decoded' into recognizable spectra. The Fourier Transform results in spectra that analysts can use to identify or quantify the material.

Procedure

The spectra were recorded using FTIR-SHIMADZU (Miracle10). The sample was placed on a crystal plate in the horizontal position such that gravity acts to make intimate contact with the cell. This ensures that energy interaction occurs at the crystal and sample interface where the bounce positions are located. Precise positioning was achieved to characterize a sample, by moving the analysis to a microscopic FTIR system which has positioning resolution on the order of 10 microns in diameter. The microscopic FTIR in the reflectance mode allows us to introduce an ATR probe right at the area of interest using microscopic optics in conjunction with the focused infrared beam. A blackbody source emits IR radiation over a range of wavenumbers, typically between 4000 and 400 cm^{-1}. The spectral measurements were the averages of 45 scans with a resolution of 16 cm^{-1} resulting in a spectra that analysts can use to identify or quantify the material.

Appendix V

3D Optical Profilometer

(Kapłonek *et al.*, 2020)

Principle

An optical profiler is a type of microscope in which light from a lamp is split into two paths by a beam splitter. One path directs the light onto the surface under test, the other path directs the light to a reference mirror. Reflections from the two surfaces are recombined and projected onto an array detector.

Procedure

In order to investigate the surface area of sodium carboxymethyl cellulose oxygen nanobubbles, analysis was carried out using an LASER PROFILOMETER - Zeta-20. Placed the sample under the lens of the loading platform, used three main optical methods (confocal, interferometry,and focus variation) and was characterized by the following properties: capacity: 700×600×40 mm;maximum vertical scanning range: 20, 100, 10 (interferometry), and 37 mm (confocal, focus variation);resolution and linearity (z-axis): 2 nm; and <0.5µm/mm linear stage.

Appendix VI

X-ray Diffraction (XRD)

(Miatmoko *et al.*, 2021)

Principle

X-ray diffraction is carried out to determine the crystallographic structure based on constructive interference of monochromatic X-rays on a crystalline sample . These X-rays are generated by a cathode ray tube, filtered to produce monochromatic radiation, collimated to concentrate and directed toward the sample.

Procedure

X-ray diffraction analysis of sodium carboxymethyl cellulose oxygen nanobubbles were analyzed by using PANalytical X'Pert Pro. Sample solutions were placed in a container and flattened and measurements were taken. This process was performed under the following conditions: Cu metal anode, Kα filter, voltage of 40 kV, 30 mA, and 2ø of 5°–90°.

Appendix VII

Assessment of Dissolved Oxygen Content

(Hu *et al*., 2018)

Principle

In an electrochemical dissolved oxygen sensor, dissolved oxygen diffuses from the sample across an oxygen permeable membrane and into the sensor. Once inside the sensor, the oxygen undergoes a chemical reduction reaction, which produces an electrical signal**.**

Reagents

1. 30% w/v H_2O_2
2. Deoxygenated Phosphate buffered saline (PBS) pH 7.4
3. 0.1 N sodium hydroxide (NaOH)
4. 37 % Hydrochloric acid

Procedure

The O_2 generated by sodium carboxy methyl cellulose oxygen nanobubbles was measured using a dissolved oxygen meter. For this, the probe of the dissolved O_2 meter is immersed to the near bottom of the flask and sealed with a rubber plug. 100 mL of deoxygenated PBS 6.5 (0.1 M) or PBS 7.4 (0.1 M) was injected. Thereafter, 30% w/v H_2O_2 was injected into the flask to obtain the H_2O_2 solution with a concentration of 100 μM. The sodium carboxymethyl cellulose oxygen nanobubbles solution was injected into the flask after the readings recorded by the detector stabilized. Moderate shaking of the flask was maintained during the experiment. The values of the dissolved O_2 detected by the probe were recorded at predetermined times.

Appendix VIII

Isolation of Lymphocytes

(Dagur, 2015)

Principle

The RBC Lysis Buffer uses an optimized concentration of ammonium chloride and enhancers to lyze the red blood cells that does not effectively lyze the nucleated RBCs. The use of RBC Lysis Buffer allows for the preferential lysis of red blood cells from whole blood as these are the majority of cells in whole blood. It also permits the concentration of the nucleated white blood cells.

Reagents

1. 10X RBC lysis buffer
2. Phosphate Buffered Saline pH 7.4 (PBS)
3. 0.1N Sodium hydroxide (NaOH)

Procedure

Venous blood was obtained from healthy volunteers. 3 mL of RBC lysis buffer (pH 7.5-8.5) was added into 1 mL whole blood, mixed gently and incubated at room temperature for 10 minutes. Centrifuged for 5 minutes at 1,600g at 4°C. Removed the supernatant. Then mixed with a 100 µL PBS buffer gently. Centrifuged at 1,600g for 1 minute at 4°C. Discarded the supernatant. Resuspended the sample with 100 µL PBS, and transferred the sample into a new 1.5 mL Eppendorf tube (EP tube).

Appendix IX

Induction of Hypoxia

(Wu and Yotnda, 2011)

Principle

Cobalt (II) Chloride hexahydrate ($CoCl_2 \cdot 6H_2O$, MW=237.9) is a chemical inducer of hypoxia. This product is soluble in water (100 mg/ml), yielding a clear, red solution.

Reagents

1. Cobalt (II) Chloride hexahydrate

Procedure

Prepared a 2.5mM stock solution in sterile distilled water, (prepared just before use).Used $CoCl_2$ at the final concentration of 50 µM in isolated cells to induce hypoxia. Added the $CoCl_2$ to cell suspension and incubated the cells for 4 hours at Room Temperature (37°C) to induce hypoxia.

Appendix X

Cell Viability Assay

(Freitas *et al.*, 2014)

Principle

Trypan blue is an azo dye that is cell membrane impermeable and therefore only enters cells with compromised membranes. Upon entry into the cell, trypan blue binds to intracellular proteins thereby rendering the cells a blue color. The trypan blue staining assay allows for a direct identification and enumeration of live (unstained) and dead (blue) cells in a given population.

Reagents

1. Phosphate buffered saline pH 7.4 (PBS)
2. 0.1N Sodium hydroxide (NaOH)
3. 37 % Hydrochloric acid
4. 0.4% Trypan blue (TB)
5. Ethanol

Procedure

1.0×10^5 PBMCs were placed in 5-mL round-bottom tubes and incubated with 190 µL PBS. To the cells, 0.4% trypan blue solution diluted in PBS was added to perform the test. Prepared samples were aliquoted into the counter slides and used for counting. Cell count and cell viability was measured both before and after the experimental set up initiation and completion respectively.Haemocytometer was used to count the approximate number of live and dead cells along with the overall cell density in the sample (Strober, 2001). Counted the total and blue cells in a Neubauer chamber.

Number of cells/ml

Total number of cells = (Total cells counted x Dilution factor x 10,000 cells/ml) / Number of squares counted.

Percentage viability

$$\text{Viable cells (\%)} = \frac{\text{total number of viable cells}}{\text{total number of cells}} \times 100$$

Appendix XI

Assessment of Hypoxia Reversal by Trypan Blue Assay

Principle

Oxygen microbubbles are similarly formulated to microbubble ultrasound contrast agents used for imaging, but comprise an oxygen gas core instead of heavy molecular weight gasses that can deliver oxygen to hypoxic cells. Synthesized oxygen microbubbles were added to acute hypoxic lymphocytes to assess whether the oxygen microbubbles can revert hypoxia.

Reagents

1. 2.5 mM cobalt chloride
2. Phosphate buffered saline pH 7.4 (PBS)
3. 0.1N Sodium hydroxide (NaOH)
4. 37 % Hydrochloric acid
5. Ethanol

Procedure

Approximately 7.0 X 10^4 lymphocytes were taken in the eppendorf tube, PBS was added to make up to 200 µl at pH 7.4. Cobalt chloride was used to induce acute hypoxia in cells at a final concentration of 0.05 mM. Various concentrations (50µl and 100µl) of SCMC-ONB were added immediately after induction of hypoxia. The cells were incubated at room temperature (37°C). Cell viability was assessed by trypan blue assay immediately after addition of SCMC-ONB and after 3 hours of incubation.